Overview and Optical Design for

DAVINCI: the Diffraction limited Adaptive optics Visible and Infrared iNtegral field spectrograph and Coronagraphic Imager

By Sean Adkins, Renate Kupke, Sergey Panteleev, Mike Pollard and Sandrine Thomas

Version 1.0
April 13, 2010

Table of Contents

Table of Contents

Figures and Tables

Figures and Tables

1 INTRODUCTION

DAVINCI, the Diffraction limited Adaptive optics Visible and Infrared iNtegral field spectrograph and Coronagraphic Imager is the first light science instrument for the Keck Next Generation Adaptive Optics system (NGAO) at the W. M. Keck Observatory (WMKO).

DAVINCI is a fully cryogenic instrument providing imaging at the diffraction limit over a wavelength range of 0.7 μm to 2.4 μm with a fixed plate scale of 8 milliarcseconds (mas). The field of view (FOV) for imaging is 32.8" x 32.8" using a Teledyne Hawaii-4RG detector with 4096 x 4096 pixels and a 2.5 μm cut-off wavelength. The imager provides a selectable coronagraph mask and a large selection of photometric, continuum, and narrow band filters. A tracking cold pupil mask is provided for H and K band observations, and an additional selection of pupil masks is provided for the shorter wavelength bands and for the coronagraph mode.

DAVINCI also provides integral field spectroscopy (IFS) with a baseline configuration of 80 x 80 spatial samples over a wavelength range of 0.7 μm to 2.4 μm. Samplings scales of 10, 35, and 50 mas are provided, resulting in an FOV of 0.8" x 0.8", 2.8" x 2.8", and 4" x 4". A deployable pick-off mirror located on axis sends the central portion of the DAVINCI FOV to the IFS. The IFS is located near an intermediate focal plane to minimize vignetting, allowing simultaneous spectroscopy and imaging. Fixed gratings are provided for each wavelength range, operating in the first order near the blaze angle with R ~4,000. The IFS is optimized for narrow band observations (~5% bandpass) and uses a lenslet image slicer combined with novel reformatting optics to provide 6 virtual slits (512 pixels per spectra) on a Hawaii-4RG detector with a 2.5 μm cut-off wavelength.

This document provides an overview of the DAVINCI instrument and describes the DAVINCI optical design.

2 SCOPE AND APPLICABILITY

This document describes the preliminary optical design for the DAVINCI fore-optics and imager, and the conceptual design for the DAVINCI integral field spectrograph (IFS).

3 REVISIONS

This revision of the document is as a template for the preparation of the report.

3.1 Revision History

Revision	Date	Author	Reason for revision / remarks
0.1	March 17, 2010	SMA	Template for report, not released
1.0	April 13, 2010	SMA	Released for review

Due to the difficulties encountered with documents using moderately complex formatting such as this one, the Microsoft Word "Track Changes" feature is not useable. To see the changes in this document since the previous revision, use the "Tools, Track Changes, Compare Documents" drop down menu sequence and compare this document to the previously released version. It is not recommended that you attempt to print the results. There is no previously released version of this document. Subsequent versions of this document will include the filename and date for the previous version.

3.2 Document Control

This is not a controlled document.

4 DAVINCI GLOSSARY

The following names and definitions are adopted for the components of DAVINCI:

DAVINCI: the complete system consisting of the DAVINCI instrument and associated computers, private network, software and accessories.

DAVINCI Instrument: the telescope-mounted portion of DAVINCI consisting of the dewar, electronics rack and interconnecting cables.

Dewar: a vacuum cryostat chamber containing the imager and integral field spectrograph science optical paths, science detectors, and associated components.

DAVINCI Instrument Electronics Rack: an EMI tight, forced air cooled EIA 19 inch equipment rack that provides a single bay with 45 U of panel space with tapped EIA 19 inch rack mounting rails. The electronics cabinet is located in the AO electronics vault on the Keck II right Nasmyth platform.

DAVINCI Computer: a computer dedicated to providing software functions for DAVINCI. There will be three of these, and they are divided into two broad categories, host and detector targets.

DAVINCI will use a client-server architecture. Low-level servers implement Keck keyword communications for clients and low level interfaces to instrument hardware to allow keyword control of the instrument. A global server is used to coordinate keyword activities by multiple low level servers. Low-level server applications can run on either the host computer or a target computer. Low-level servers that demand significant amounts of processor resources are often deployed on dedicated computers; these are commonly called target computers. The host computer is the computer where the user interface applications are run, even though this same computer may also run on or more of the server applications as well.

DAVINCI Target Computer: a computer dedicated to running one or more low-level server applications that provide keyword control of DAVINCI hardware systems. A target computer has one or more hardware interfaces to subsystems of the instrument such as detectors or mechanism motion control.
DAVINCI Host Computer: the computer where the DAVINCI global server and user interface software is run.

DAVINCI Computer Rack: an EIA 19 inch rack located in the Keck II computer room and housing the DAVINCI computers, data storage disk array, private network interfaces and related components.

5 OVERVIEW

5.1 Science Drivers

DAVINCI is expected to offer high performance imaging and spectroscopy for science observations with NGAO. The top level science driven requirements for DAVINCI are:

1. Diffraction limited imaging from 0.7 to 2.4 µm with at least 3 pixel sampling to 1 µm, and 2 pixel sampling to 0.7 µm
2. High throughput
3. Imaging over an FOV that is as large as possible for NGAO, ~20" to 30" diameter
4. Integral field spectroscopy from 0.7 to 2.4 µm with spatial scales suited to the diffraction limit and the maximum ensquared energy provided by NGAO
5. Coronagraphic imaging with contrast of at least 10^{-4} from 1 to 2.4 µm over an inner working angle of 200 mas

NGAO offers a significantly extended parameter space for these observations, both in terms of spatial resolution and wavelength range. Figure 1 illustrates this parameter space.

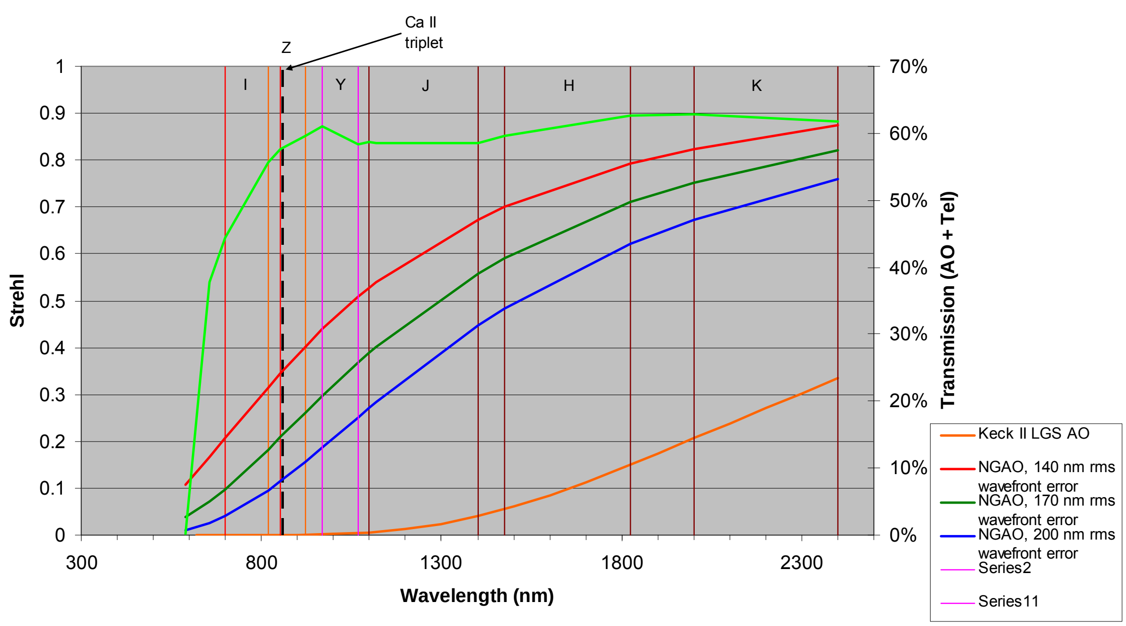

Figure 1: NGAO parameter space

The performance expected from the NGAO system (Dekany et al., 2009) includes average Strehls of at least 15% in the I band and performance of ~78% in the K band, assuming 170 nm rms of residual wavefront error. Detailed studies of the performance for various science cases and sky coverage fractions support the view that imaging capability suited to the diffraction limit will provide excellent results over the wavelength range of 0.7 to 2.4 μm. The combination of the AO system and imaging capability are expected to support high accuracy relative photometry and high accuracy astrometry. The imaging capability is also expected to have high throughput and appropriate background suppression in order to take advantage of the low backgrounds provided by NGAO, and the imaging capability must provide a coronagraph to support the detection and characterization of planets around nearby low mass stars.

An integral field spectrograph (IFS) is recognized as an ideal way to take advantage of the image quality offered by NGAO because of its ability to provide spatially resolved spectroscopy of diffraction limited images without suffering from losses due to a mismatch between a long slit and the shape of a complex object. IFS data can provide information essential for deconvolution of the point spread function (PSF) and offers a comprehensive tool for determining kinematics, mass distributions and velocity dispersions.

5.1.1 Imaging Science with DAVINCI

DAVINCI's imaging capability represents a general purpose tool that will be expected to serve a wide range of scientific needs as well as provide a tool for characterizing the performance of the NGAO system. The imager's performance requirements are in turn defined from two viewpoints, the NGAO science cases, and a technical viewpoint that defines the requirements for performance measurement. Here we will consider the science driven performance requirements with an understanding that satisfying the most demanding of these will also provide the performance needed for AO system characterization.

The general purpose nature of the imaging capability is reflected in the number of NGAO science cases that require imaging. Based on a review of those science cases, the important performance parameters for the imaging capability are summarized by science case in Table 1.

Several of these science cases identify the desirability of accessing wavelengths below 1 μm, either for specific diagnostic lines such as the Ca II triplet (~850 nm), or for the improved spatial resolution available at the shorter wavelengths. A number of the science cases also require high levels of performance from astrometric and photometric measurements obtained from NGAO observations. Initial evaluation of the I band for color-color diagrams indicates that extending coverage to this band will prove highly beneficial to the study of stellar populations.

Science Case	Wavelength Coverage†	Field of View	Spatial Sampling	Sensitivity and SNR	Other requirements
Measurements of General Relativity Effects in the Galactic Center*	H, K (1.49 to 2.37 μm)	10" x 10"	At least λ/2D sampling	Better than current AO system with NIRC2	Astrometric performance > 0.1 mas
Imaging and Characterization of Extrasolar Planets around Nearby Stars*	Y, J, H, K (0.97 to 2.37 μm) Also below Y to 0.9 μm	< 5"	Diffraction limited sampling. At least 1.5 x better than λ/2D sampling at J (goal Y)	10^{-4} contrast at 200 mas separations, goal of coronagraph with inner working angle of 70 to 100 mas. ΔH = 13 at 1" separation, H = 25 for σ = 5 in 20 minutes.	R ~100 spectroscopy? Relative photometry to accuracy ≤ 0.1 magnitudes, astrometric precision of 2 mas. 6 λ/D general purpose coronagraph.
Multiplicity of minor planets*	Z, Y, J, H, K (0.818 to 2.37μm)	≤ 4"	Diffraction limited, λ/3D for J, H, and K-bands, or λ/2D for R and I-bands		
Gravitational Lensing	I, Z, Y, J, H, K (0.7 to 2.37 μm)	≥ 15" dia., goal of 30" dia.	Diffraction limited, λ/2D		Relative photometry to accuracy ≤ 0.1 magnitudes
Size, shape, and composition of minor planets	Z, Y, J, H, K (0.818 to 2.37 μm) I band to 0.7 μm desirable for asteroid shapes	≤ 4"	Diffraction limited, λ/3D for J, H, and K-bands, or λ/2D for R and I-bands	R = 29 for 5σ in 1 hour (from NGAO proposal, table 14)	R ~100 spectroscopy?
Characterization of Gas Giant Planets	J, H, K (1.17 to 2.37 μm)	≥ 30" dia. in K, ≥ 20" dia. in J,H	Diffraction limited, λ/2D or finer sampling	Moons are very bright, need a large dynamic range, short exposures	
Resolved Stellar Populations in Crowded Fields	I, Z (0.7 to 0.922 μm), J, H, K (1.1 to 2.37 μm)	≥ 15" dia.	Diffraction limited, λ/2D or finer sampling	K = 27 for σ = 5 in one hour	

Table 1: Summary of the primary science driven parameters for DAVINCI imaging

** = NGAO key science driver*
† = Photometric filter passbands

Photometric accuracy depends strongly on the stability of the point spread function (PSF). For observations of closely spaced targets, accurately modeling the PSF becomes critical to successfully employing deconvolution techniques to separate the flux contributed by each object. Britton et al. (2007) suggest that effects due to imperfect correction of atmospheric turbulence and field dependent aberrations will be dominant over effects due the instrumentation. Non-common path errors between the science instrument and the AO system will contribute to instability of the PSF at the instrument. Motion within the instrument structure during an observation (flexure) can also contribute to PSF variability. Flexure is not expected to be a problem for DAVINCI as its structure is completely fixed, and there are no moving parts that can induce differential motion between parts of the optical path during an observation. We will not attempt an extended discussion of the instrumental contributions to photometric accuracy, but detector characteristics are expected to be the dominant factor in the instrument's photometric performance. Such effects are well understood and largely controllable with good design practices.

The accuracy of position determination or astrometry for a point source is ultimately determined by the width of the PSF and noise in the image due to photon statistics, sometimes referred to as the photonic limit. As with photometric accuracy, the performance of the AO system, including the Strehl and the quality of the PSF both affect the signal to noise ratio (SNR) of the observation. As discussed in Cameron et al. (2007) additional impacts on astrometric accuracy arise from AO performance issues such as variable angular displacement across the FOV due to differential tip-tilt anisoplanatism, and changes in plate scale that may result from blind modes in multi-conjugate AO (not currently a planned operating mode for the NGAO system).

In addition to sensitivity, the primary effect of the instrument on astrometric accuracy will be the amount of distortion present in the optical system. In addition to minimizing the presence of distortion through careful design and construction a high performance approach to measuring the distortion across the field of the imager will be required. Such characterization has been shown to have a significant impact on the astrometric accuracy that can be achieved with the existing Keck II AO system and the NIRC2 instrument (Cameron et al., 2007). It should be noted that the Galactic center case makes the greatest demand on astrometric accuracy at < 0.1 mas, an accuracy approaching the limit of what can be achieved due to photon statistics.

The pixel scale at the detector will determine the sampling of the delivered PSF and in turn will have an impact on both photometric and astrometric accuracy. The effects of sampling on the spatial frequency content of the PSF image can be appreciated using the techniques common to understanding the MTF of digital imaging systems. The loss of spatial frequencies due to sampling will translate directly to a reduction in the accuracy with which the original flux distribution is represented in the sampled image, and will also result in an increase in position uncertainty for well resolved image features.

For the specific case of imaging of multiple asteroid systems Baek and Marchis (2007) have undertaken simulations which indicate that pixel scales resulting in three pixel sampling across the diffraction limited image size (a pixel scale of $\lambda/3D$) results in the best representation of the flux ratio between the primary and the secondary in the J, H and K bands. For near-IR wavelengths for which the chosen object sizes are well resolved (J and H band) Baek and Marchis also report that three pixel sampling produces good results for position measurements. In the I band the shorter wavelengths offer higher spatial resolution, but the decrease in Strehl reduces the SNR of the simulated observations, and as a result two pixel sampling (a pixel scale of $\lambda/2D$) provides the best representation of the flux ratio and the most accurate position measurements.

5.1.1.1 Imager Pixel Scale

For reasons of complexity, optical performance, and cost we consider it desirable for the DAVINCI imaging mode to have a single fixed pixel scale. Given square detector, the square area that will fall entirely within a 40" FOV is 28.28" x 28.28". Given a 4096 x 4096 pixel detector, the corresponding pixel scale is 7 mas. A second candidate is an 8 mas scale, which provides a FOV of 32.8" x 32.8". As noted in the previous section, the imager should have a pixel scale that provides at least 3 pixel sampling in the near-IR bands, and at least 2 pixel sampling in the Z and I bands. The sampling obtained in each waveband for pixel scales of 7 and 8 mas is illustrated in Figure 2.

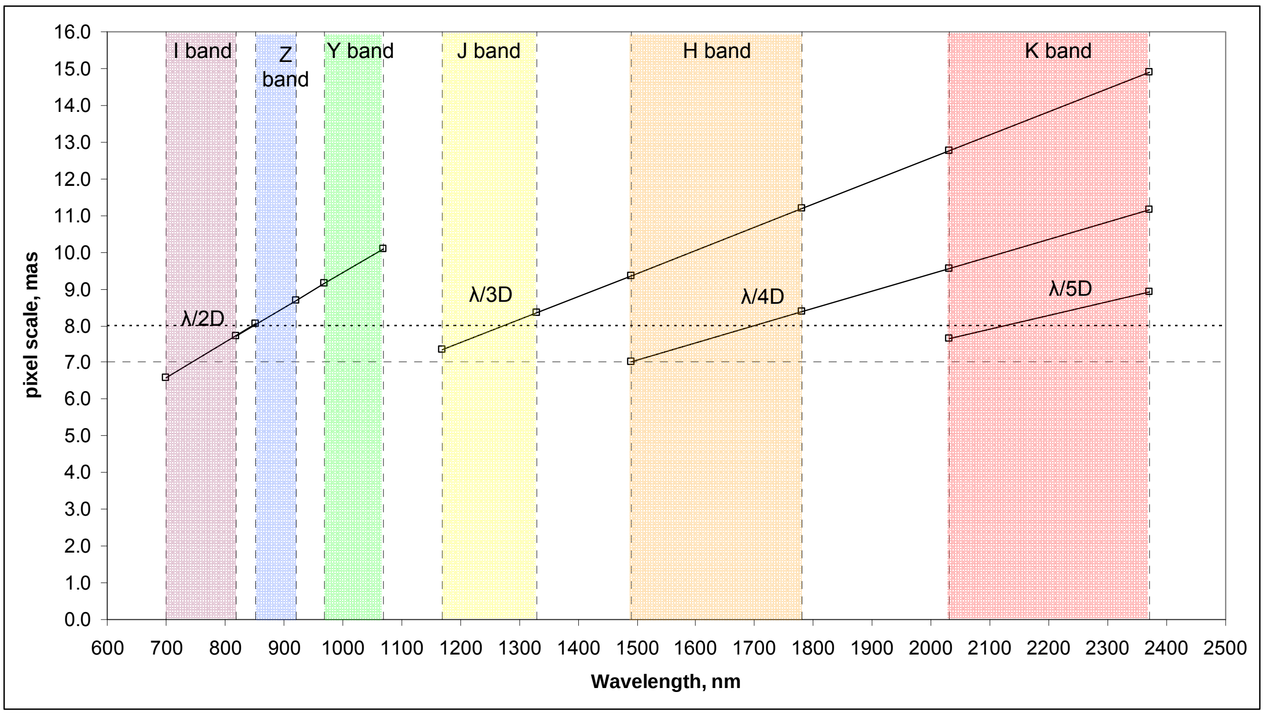

Figure 2: DAVINCI photometric wavelength bands and spatial sampling

From Figure 2 we can see that a 7 mas pixel scale would provide >2 pixel sampling down to near the I band cut-on wavelength, >2 pixel sampling in the Z and Y bands, >3 pixel sampling in the J band, ≥ 4 pixel sampling in H, and > 5 pixel sampling in K band. An 8 mas pixel scale would provide 1 to 2 pixel sampling in I band, >2 pixel sampling in the Z and Y bands, 2 to 3 pixel sampling in the J band, 3 or more pixel sampling in H, and 4 to 5 pixel sampling in K band. The benefit of the 8 mas pixel scale would be an increased FOV.

The trade off between pixel scale and background limited exposure time has been evaluated for a range of pixel sizes. As shown in Figure 3, smaller pixels receive less background per pixel, but as can also be appreciated more pixels also increase the read noise contribution. Fortunately the Hawaii-2RG detector has demonstrated read noise of ~4 e- with 16 Fowler samples (Kulas, 2010), considerably reducing the impact of oversampling due to a fixed pixel scale.

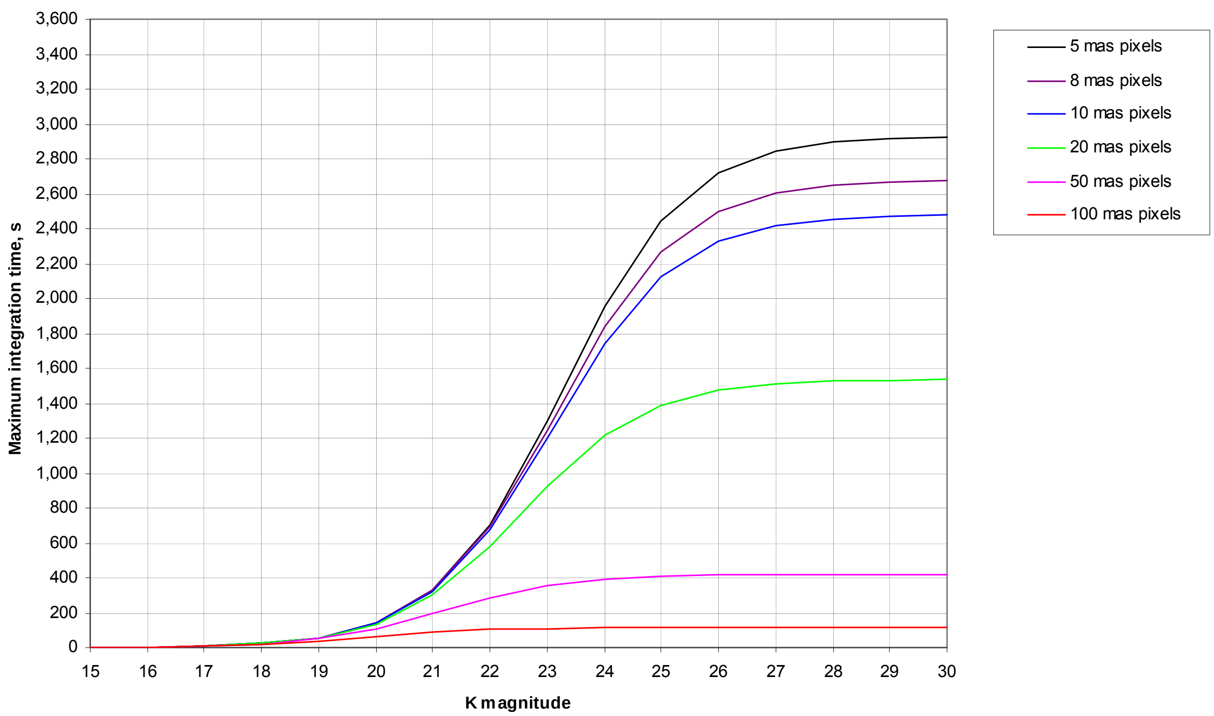

Figure 3: Maximum exposure time to 50% of charge storage capacity in K band

When the benefits of the smaller pixel scale to spatial resolution, and having evaluated a number of scales from 5 mas to 50 mas for the trade off between the limit imposed by the sky background on the maximum exposure time and the benefit of the increased FOV a pixel scale of 8 mas has been selected for the DAVINCI imager.

5.1.1.2 Imager Sensitivity

The imager photometric passbands, zero points, and background predictions for DAVINCI imaging are shown in Table 2. The sensitivity predictions for DAVINCI imaging are shown Table 3. The background predictions are based on a cooled AO system operating at a temperature of -15 °C and emissivity for the LGS observing mode assuming degraded optical transmission due to dust and aging of coatings. The background predictions include the effects of moonlight (50% dark time) for the I and Z band. Average transmission in each passband is used for the atmosphere, telescope, and AO system. The values for these transmissions are given in appendix B. The DAVINCI imager transmission values for each passband are shown in Table 12. Thermal background within DAVINCI is suppressed by operating the instrument at 120 K in a vacuum dewar.

The zero point magnitudes and the sensitivity predictions (Table 3) are based on the detector characteristics summarized in Table 4. Sensitivities are calculated assuming the delivered NGAO Strehl based on 170 nm wavefront error. The required aperture for a diffraction limited image is assumed to be that needed for a well compensated image (Hardy, 1998, p. 42), i.e. a diameter equal to $2\lambda/D$ where D is the diameter of the telescope aperture, and λ is the long wavelength cut-off in the passband of interest.

.

Table 2: Zero points and background magnitudes for DAVINCI imaging

Photometric Passband	Cut-on, nm	Cut-off, nm	CWL, nm	Zero point	Background, mag./sq. arcsecond
I band photometric	700.00	853.00	776.50	27.45	22.13
Z band photometric	818.00	922.00	870.00	27.28	21.28
Y band photometric	970.00	1070.00	1020.00	27.04	17.28
J band photometric	1170.00	1330.00	1250.00	27.11	16.04
H band photometric	1490.00	1780.00	1635.00	27.13	13.76
K band photometric	2030.00	2370.00	2200.00	26.57	14.78

Table 3: DAVINCI imaging sensitivity

Photometric Passband	Ave. Strehl (170 nm wavefront error)	Time per exposure	5σ mag.	Time for single exposure to background limit, mag. = 27
I band photometric	15%	120 s	27.8	6.7 h
Z band photometric	22%	120 s	27.9	5.6 h
Y band photometric	33%	900 s	28.0	1800 s
J band photometric	39%	900 s	27.4	560 s
H band photometric	59%	900 s	26.5	70 s
K band photometric	79%	900s	26.7	280 s

Point source limiting magnitude for 4 co-added exposures to reach 5σ in 1 hour for Y through K bands, and 8 minutes for I and Z bands

Table 4: Hawaii-4RG performance parameters

Parameter	Goal Value	Notes
Dark Current	0.01 e^-/s	Median dark current of all imaging pixels
Charge Storage Capacity	100,000 e^- /pixel	Array average number of electrons where the photon transfer curve first deviates from a straight line
Read Noise	15 e^-/pixel	Per CDS read
Quantum Efficiency	0.80 0.75 0.70	970 to 2400 nm 850 to 970 nm 700 to 850 nm

5.1.2 Spatially Resolved Spectroscopy Science with DAVINCI

DAVINCI's IFS capability is intended to meet the needs of a range of Galactic and extra galactic science observations. We have evaluated the key IFS performance parameters and determined that the parameters most critical to IFS science are wavelength coverage including the placement of the short wavelength cut-off, spectral resolution, FOV, spatial sampling, and sensitivity. Table 5 gives the values of these parameters for each of the science cases that represent the primary drivers of IFS performance for DAVINCI.

Science Case	Wavelength Coverage	Spectral Resolution	Field of View	Spatial Sampling	Sensitivity and SNR
Galaxy Assembly and Star Formation History*	Z, Y, J, H, K (0.818 to 2.4 μm), narrow band coverage acceptable since redshifts will be obtained before IFS observations	R >3000 (for OH line removal and discrimination of key diagnostic lines (Hα vs. NII)	1" x 3" or greater	Optimized for 50% ensquared energy, range of 50 to 100 mas acceptable	K band performance improvements needed (lower background). Seeking 5 times better sensitivity than OSIRIS on current Keck AO system
Nearby Active Galactic Nuclei*	Z, Y, J, H, K (0.818 to 2.4 μm, or at least to below 850 nm for the Ca II triplet)	R ~3000 to 4000	≥ 5" dia.	20 mas in the near-IR, 8.5 mas in Z	High spatial resolution and precision radial velocities
Measurements of General Relativity Effects in the Galactic Center*	H, K (1.475 to 2.4 μm), primarily narrow band observations of specific absorption lines	R ~4000	≥ 5" dia., goal of 10" dia.	20 mas (H band) and 35 mas (K band)	RV precision at least 10 km/s
Gravitational Lensing	I, Z (0.7 to 1.05 μm), J, H, K (1.10 to 2.4 μm)	R ~4000	> 4" dia., goal of 8" to 10" dia.	50 mas or smaller	RV precision at least 20 km/s (1 σ)

Table 5: Summary of the primary science driven parameters for an IFS

** = NGAO key science driver*

In the IFS design one of the key performance trades is the relationship between spectral coverage, spectral sampling, and FOV. For a given number of detector pixels one can trade between these three parameters, finding that certain combinations are more efficient in using the available detector area than others. Our analysis indicates that the NGAO science cases requiring IFS observations are generally more concerned with obtaining a larger FOV than they are with full coverage of an entire IR or visible passband in one exposure.

For example, the Galactic Center case emphasizes the measurement of absorption lines in the H and K bands (such as HI absorption of Brγ emission at 2.166 μm) that fall within 5% band passes, while FOVs of 5" diameter are desirable for simultaneous measurements of multiple stars near the

Galactic center to improve the strength of the orbital solutions. Measurements of GR effects at the Galactic center demand high SNR and diffraction limited spatial sampling. FOV and sensitivity are also important for population studies at the Galactic center (Lu et al., 2009).

Similarly, for emission line observations such as excitation temperatures, observations of molecular hydrogen emissions (Beck et al., 2008), and other spectral line features such as the CO bandheads, 5% band passes will suffice. For the galaxy assembly and star formation case the primary requirement is sensitivity, while FOV is less important provided that it is large enough that sufficient spatial pixels are available to accurately sample the sky background. For this science case since the targets are of known redshifts, and the key spectroscopic lines of interest for kinematics at redshifts of $1 < z < 3$ are observable within ~5% passbands in the near-IR (J, H, and K) bands, a narrow band pass is also satisfactory.

Because the solution for black hole mass requires having a good model for the larger-scale structure of the galaxy the nearby AGN science case has a need for larger FOVs of 3" to 5" diameter, but again the observations required for the stellar and gas dynamics around the central black hole are based on absorption lines for stellar dynamics and emission lines for gas dynamics, all of which can be observed within 5% band pass or less in the z through K bands. This science case in particular identifies the benefits of high angular resolution observations below 1 μm wavelength where the more compact PSF core at the shorter wavelength and the reduced sky background will enable BH detection over greater distances. Gravitational lensing also requires high SNR and an FOV of at least 4" to 5". The lensing science case can also benefits from observations below 1 μm for access to diagnostic lines for the lensed source and for red shifted lines of the lensing galaxy.

In cases where observations of multiple lines are required, if the IFS field is suitably matched to the object size, such that the entire PSF of the object is imaged, then image motion can be detected and discounted using simple PSF fitting techniques (Roth, 2006). This allows multiple narrow band exposures to be a practical alternative to a single broad band exposure.

5.1.2.1 IFS Sensitivity

The predicted sensitivity for the DAVINCI IFS is shown in Table 6. This table is based on the predicted transmission of the IFS, and the assumptions for Strehl, atmospheric transmission, background, and detector as described in §5.1.1.2.

Table 6: Zero points and background magnitudes for DAVINCI IFS

Passband	Cut-on, nm	Cut-off, nm	CWL, nm	Zero point	Background, mag./sq. arcsecond
I band spectroscopic	700.00	853.00	776.50	26.55	22.13
Z band spectroscopic	855.00	1050.00	952.50	26.95	20.68
Y band spectroscopic	970.00	1120.00	1045.00	26.53	17.05
J band spectroscopic	1100.00	1400.00	1250.00	26.93	16.33
H band spectroscopic	1475.00	1825.00	1650.00	26.43	13.79
K band spectroscopic	2000.00	2400.00	2200.00	25.88	14.62

5.2 Design and Build to Cost

DAVINCI originates within the design and build to cost requirement for NGAO, and is based on a design and build to cost approach supported by six principles:

1. Ensure that the instrument capabilities are well matched to key science requirements
2. Ensure that the instrument capabilities are matched to the to AO system in order to maximize the science gains
3. Understand which requirements drive cost
4. Resist the temptation to add features
5. Maximize heritage from previous instruments
6. Evaluate ways to break the normal visible/near-IR paradigm of using different detectors in separate instruments

The concept developed for DAVINCI is aimed at satisfying principles 1 and 2 as fully as possible. The main aspects of the concept as described here are then intended to address the remaining principles with a clearly cost driven approach supported by sound engineering and technical decisions. The design adopts significant portion of subsystem designs from previous instruments, in particular the MOSFIRE (McLean et al., 2008) and OSIRIS (Larkin et al., 2006) instruments. To meet the cost requirements DAVINCI incorporates two instrument capabilities (imaging and spectroscopy) in a single cryogenic dewar with common fore-optics. The single dewar offers significant cost savings by eliminating the need to duplicate the dewar itself as well as cryogenic cooling and a number of control and supervisory systems such as temperature control and pressure monitoring.

A second important aspect of the design concept addresses principal 6, and that is the use of substrate removed HgCdTe infrared focal plane arrays (FPAs). The substrate removed FPAs have good (~70%) QE down to 500 nm, and although the single CDS read noise is higher than typical science grade CCDs (~15 e^-/read for a Hawaii-2RG vs. 5 e^-/read for a deep depletion CCD, see Adkins, 2009) the low power dissipation of the FPA read out integrated circuit and non-destructive pixel read out allows many Fowler or up the ramp samples and results in essentially the same readout noise levels for exposures where the exposure duration allows time for the required number of reads. The result is that while the QE of CCDs will be at least 20% higher at 1 μm and below, this seems to be the only penalty for not using a CCD below 1 μm. This represents another important component of the cost reduction needed in order to ensure that DAVINCI supports the NGAO design and build to cost requirement.

5.3 The DAVINCI Concept

A block diagram of DAVINCI is shown in Figure 4. DAVINCI is a fully cryogenic infrared and optical (to 0.7 µm) imager and IFS enclosed in a vacuum dewar. The dewar contains two optical systems, one for the imager shown in the upper portion of the block diagram, and one for IFS, shown at the bottom center of the block diagram. The FOVs of the imager and IFS are both at the center of the NGAO science FOV as illustrated in Figure 5.

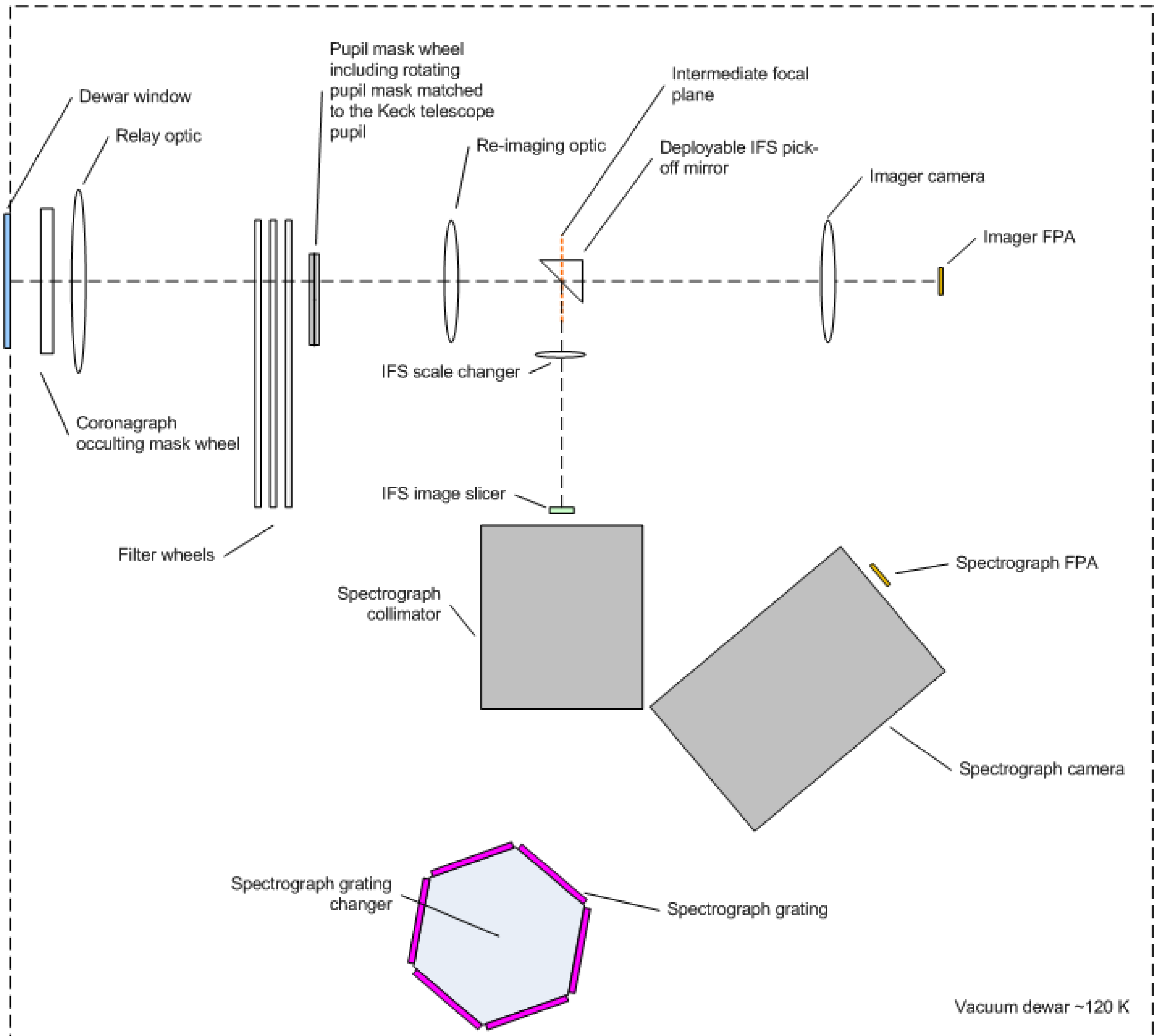

Figure 4: DAVINCI opto-mechanical block diagram (not to scale)

Starting at the top left side of the block diagram, light enters the dewar from the AO system through a vacuum window ~ 90 mm in diameter. The window is coupled to the NGAO system's cooled enclosure via a light and air tight bellows. The bellows isolates the two structures mechanically, and since the AO enclosure is cooled to -15 °C and filled with dry air, the emissivity of the window is reduced and the issue of condensation or ice on the window is eliminated during normal operation. A mechanism such as a dry air purge will need to be provided for the window during servicing or testing to prevent condensation when the window is exposed to ambient conditions.

The AO system's science focal plane is located inside the dewar where a wheel is located providing a selection of coronagraph occulting masks. A relay optic forms a pupil image at a wheel carrying a selection of cold pupil masks for imaging and coronagraphy including a tracking pupil mask matched to the primary mirror aperture and central obscuration of the Keck telescope.

A set of filter wheels is located just in front of the pupil plane, with ~45 filters shared between the imager (24) and the IFS (17). Each wheel will contain ~15 filters plus an open position. After the pupil mask a re-imaging optic forms an intermediate focal plane. Continuing to the right along the imager optical path this intermediate focal plane is followed by the imager camera and detector.

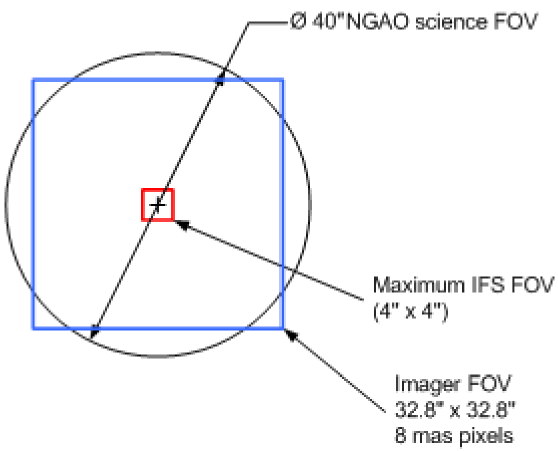

Figure 5: DAVINCI FOVs

Returning to the center of the diagram, the optical path to the IFS starts with a deployable pick-off mirror located near the first intermediate focal plane. This mirror sends the center of the intermediate focal plane to the IFS shown at the bottom center of the block diagram. The beam enters the IFS scale changer, which has three selectable scale changing optics to provide three spatial sampling scales for the IFS. The scale changer focuses the light on the IFS image slicer (baselined as a 80 x 80 lenslet array) and is then collimated by a three mirror anastigmat (TMA). The collimator TMA illuminates a grating working in the first order, and the dispersed light is then imaged onto the spectrograph detector by a second TMA. Multiple gratings will be used with a rotary grating changer to select the appropriate grating for each waveband.

5.3.1 Mechanical Design Concept

The key mechanical design feature of the NGAO science instrument is the re-use of the MOSFIRE dewar design. This may seem like an unusual choice but with appropriate modifications the concept has several benefits. First, the MOSFIRE dewar design represents a known cost with demonstrated thermal performance. Second, the dewar has a shape that minimizes deflection of the dewar walls, and is easily adapted for a fixed gravity orientation with the major axis of the dewar horizontal. Design details of the MOSFIRE dewar and internal structure may be found in the project's detailed design report ("MOSFIRE," 2007).

5.3.1.1 Dewar and Internal Structure

The MOSFIRE internal structure design is shown in Figure 6, taken from Figure 31 of the MOSFIRE detailed design report. The outer most portion of the structure is the composite support tube that provides a thermal stand-off for the instrument's internal structure. The front bulkhead (bulkhead A in the Figure) provides one of two main optical benches for mounting MOSFIRE's opto-mechanical systems. Bulkhead A is connected to a second bulkhead (bulkhead B) by a central tube and an outer support tube, these create a rigid structure that is essential to reduce flexure in MOSFIRE's variable gravity operating environment at the Keck I Cassegrain focus. Bulkhead B is the second main optical bench for MOSFIRE's opto-mechanics, and supports a continuation of the central support tube to a third smaller bulkhead where the MOSFIRE flexure control system (FCS) is mounted.

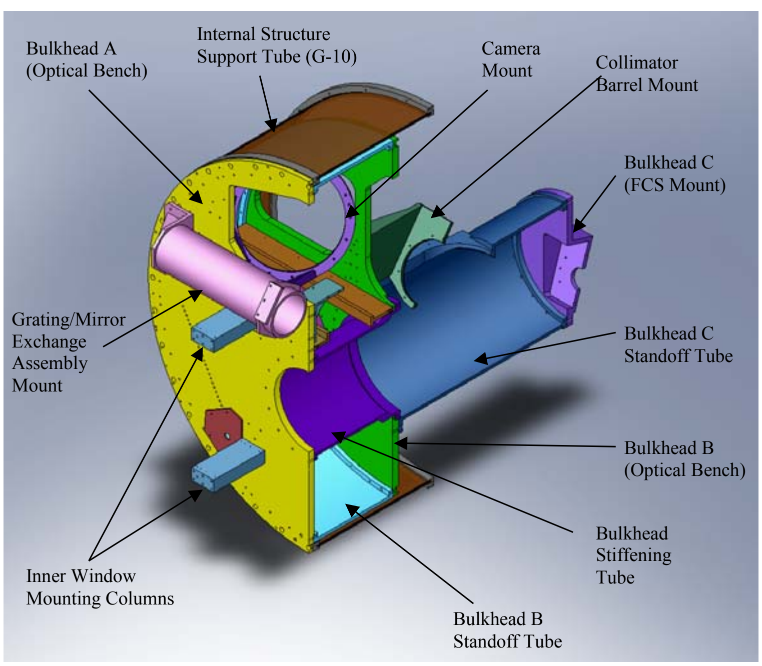

Figure 6: MOSFIRE internal structure (cross section)

The DAVINCI adaptation will eliminate the central support tube, the extension of the tube from bulkhead B, and bulkhead C. Most or all of bulkhead A will be eliminated, depending on the requirements for support of the IFS TMAs. The outer stand-off tube may need to be stiffened by additional structure to allow it to interface to the composite stand-off and support bulkhead B which will become the main optical bench for the instrument. The various other opto-mechanical support components shown in Figure 6 will be eliminated and the main optical bench layout will then be developed to match the requirements of the NGAO instrument's opto-mechanical systems.

There are some features of the MOSFIRE dewar design that are not needed. The NGAO instrument configuration will have the input light entering from a port on the side of the dewar rather than the front end cap, and the vacuum ports currently located on the front cap, which becomes the top cap, will be relocated to the rear cap. This will make the top cap a featureless dome shape. The rear cap will also be modified to eliminate the extension for the MOSFIRE FCS.

The baseline for the instrument's cryogenic cooling system will be to reuse the MOSFIRE design which employs two Brooks Automation (formerly CTI) model 1050 single stage closed cycle refrigerator (CCR) heads for cooling the dewar interior. The MOSFIRE detector is cooled by a model 350 two stage cold head, and two such cold heads will be required for the NGAO instrument. MOSFIRE is also equipped with a temperature stabilization system and uses variable speed drive for the cold heads. These features are also baselined for the NGAO instrument.

5.3.1.2 Mechanisms

The majority of the mechanisms required for the NGAO instrument can be implemented using straightforward rotary or wheel designs derived from the MOSFIRE and OSIRIS instruments. Referring to Figure 4 these include wheel mechanisms for the filters, coronagraph pupil apodizers, and coronagraph occulting masks. The instrument's two detectors may be equipped with focus mechanisms derived from MOSFIRE's detector head assembly as well. While the AO system will maintain the focus for the instrument, there are integration and test advantages to being able to shift the detector focus, and it may be important for observing efficiency to maintain parfocality between the imager and IFS channels.

The scale changer mechanisms may also be implemented using a wheel design, but the instrument's wavefront error and pupil quality requirements may make these designs more demanding, and another design approach may have to be considered.

The three mechanisms that are unique to the NGAO instrument are the pupil mask rotator, the IFS pick-off mirror deployment mechanism, and the spectrograph grating changer. The design for the pupil mask rotator will depend on the size of the pupil mask that results from the preliminary optical design. At present it appears that the pupil mask will be relatively small. Another consideration is the possibility that various sizes of pupil mask may be needed for different wavelength bands. The simplest choice is likely to be a single mask, matched to the Keck telescope pupil and rotated by a micro-stepping drive using a cryogenic stepper motor.

The IFS pick-off mirror mechanism does not need to become too challenging, the tolerances on its motion can be relaxed by making the pick-off mirror oversize and by making the axis of deployment motion parallel to the angle for the mirror's surface that is needed to direct the input beam to the IFS. However, one advantage to having a mirror close to the required size for the 4" x 4" area of the focal plane is that vignetting of the imager will be reduced, allowing the possibility of simultaneous imaging and spectroscopy. Deployment of the IFS pickoff mirror can be accomplished with either a rotary mechanism or a linear slide mechanism. Cryogenic linear stages are available, and the load requirements will be modest. The exact angle of the fold introduced into the beam by the pick-off mirror will be determined by the preliminary optical design and opto-mechanical layout considerations, but this should not have a significant impact on selection of a mechanism for the pick-off mirror.

The third mechanism unique to the NGAO instrument is the grating changer. The proposed mechanism for this is a rotary turret carrying the gratings on an outer radius. Each grating can be mounted with precision adjustments to ensure proper alignment in the spectrograph. The requirements on positioning of the gratings will be demanding in order to ensure repeatability of instrument wavelength calibrations. It is likely that this motion axis will require high precision position encoding, perhaps by using either a series of LVDTs, or perhaps optical position sensing.

It should also be noted that all motors used in the mechanisms will require proper cold strapping and shielding to prevent thermal radiation into the optical path. It is expected that motors will be energized only during mechanism moves.

5.3.2 Interfaces

The mechanical interfaces between the NGAO instrument and the telescope/AO system will be simple, provided that analysis of the stability of the mounting of the instrument and the AO system to the Nasmyth platform will support the requirements for relative motion between the instrument and the AO system. This is understood to be primarily driven by the NGAO astrometry error budget.

The instrument will mount to the Keck II telescope left Nasmyth platform on kinematic mounting pads to allow adjustment of the instrument's position for alignment with the AO system's science focal plane. The dewar will be supported by a steel tube structure that mounts to the bottom of the dewar shell's main cylinder. This corresponds to the location where the MOSFIRE dewar is mounted to the Cassegrain rotator module using an offset steel web structure.

The interface to the AO system's bench enclosure that is used to insulate the cooled bench from the dome ambient will be accomplished by a bellows. This may require insulation or be of double wall construction to ensure the integrity of the AO system's interior.

5.3.3 Electronics

DAVINCI's instrument electronics are derived directly from the MOSFIRE electronics design. An electronics rack cooled by a liquid to air heat exchanger will be mounted the AO electronics vault and will contain all of the electronics systems required by the instrument. A block diagram of DAVINCI's electronics is shown in Figure 7.

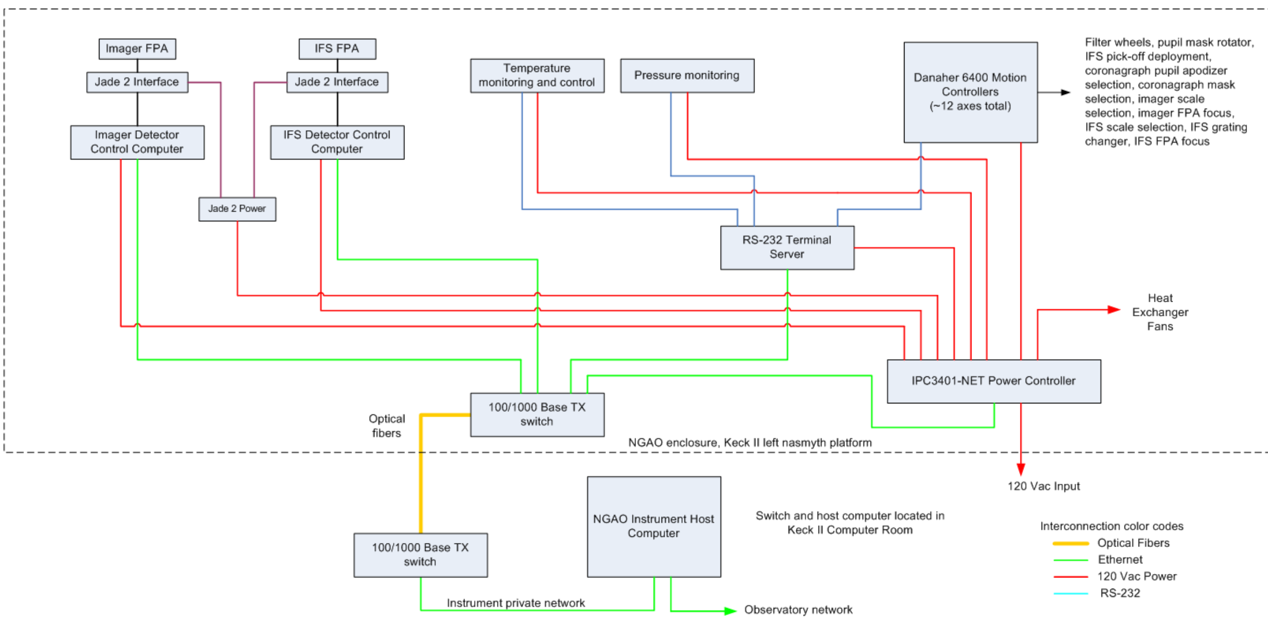

Figure 7: DAVINCI electronics block diagram

5.3.4 Software

DAVINCI's instrument software will be based on the software developed for the MOSFIRE instrument. The detector software, temperature and pressure monitoring, power controller and 6400 series motion controller software will be a straightforward port from MOSFIRE. The low level and global server architecture will also be re-used from MOSFIRE. The instrument graphical user interface (GUI) designs are TBD, but they could easily be based on a port of the MOSFIRE desktop and control GUIs.

6 OPTICAL DESIGN

6.1 Design Drivers and Choices

The concept for the DAVINCI instrument establishes the following drivers for the optical design:

1. DAVINCI will function as a visible and near-IR imager with a coronagraph, and as an IFS.

2. The first focal plane of the instrument must be able to accommodate a wheel with a number of masks to be used in coronagraphy.

3. DAVINCI must include a selection of cold pupil masks, located at a pupil image, including a tracking pupil mask matched to the shape of the Keck telescope's primary mirror.

4. For ease in manufacturing of the masks the pupil on the cold stop should be no smaller than 25mm.

5. The imager detector will be a Hawaii 4RG with 4096 x 4096, 15 μm pixels for a detector area of 61.4 mm x 61.4mm.

6. The FOV imaged onto the H4RG is 40" diameter

7. The IFS should provide sampling scales of 10 mas, 35 mas, and 50 mas.

8. The mechanical package of DAVINCI, including all optics, mechanics, and detectors, should fit in a dewar based on the MOSFIRE dewar design with appropriate modifications for a fixed gravity orientation.

The optical design also reflects specific choices that implement the design and build to cost requirement of NGAO. First, the three operating modes of DAVINCI share a common pupil image for placement of the cold stop or Lyot stop. Second, after the first pupil relay, an image plane will be produced in which the central 5" of the FOV are passed to the IFS. It is desirable that the imager and IFS can be used simultaneously (the imager, in this mode, is not required to see the central 5" that has been directed to the IFS).

6.2 Optical Performance Goals

Table 7 gives the optical performance goals for DAVINCI. These requirements are derived from the science drivers discussed in §5.1 and the 30 nm rms of uncorrectable (non-common path) wavefront error allocated to the science instrument in the NGAO flowdown budget.

Table 7: DAVINCI optical performance goals

Parameter	*Goal*	*Min.*	*Max.*	*Units*	*Notes*
Image quality					
Imager rms spot radius	≤ 1.22	-	1.22	λ x f/#	1
IFS	> 80	70	-	% ensquared energy	2
Wavefront error					
On-axis	<30	-	30	nm, rms	3
Off-axis	<60	-	60	nm, rms	4
Distortion					
Imager	< 0.25	-	0.5	%, peak to peak	5
Optical throughput					
Imager					
I band	> 60	50	-	% at 0.78 µm	6
Z band	> 70	60	-	% at 0.87 µm	6
Y band	> 70	60	-	% at 1.00 µm	6
J band	> 70	60	-	% at 1.25 µm	6
H band	> 70	60	-	% at 1.64 µm	6
K band	> 60	55	-	% at 2.2 µm	6
IFS					
I band	> 40	30	-	% at 0.78 µm	7
Z band	≥ 50	40	-	% at 0.87 µm	7
Y band	≥ 50	40	-	% at 1.00 µm	7
J band	≥ 50	40	-	% at 1.25 µm	7
H band	≥ 50	40	-	% at 1.6 µm	7
K band	> 40	40	-	% at 2.2 µm	7
Non-uniformity					
Imager	< 5	-	10	%, peak	8
IFS	< 5	-	10	%, peak	8
Instrument background					
Y-band	< 0.001	-	0.02	e^-/sec/pixel	9
J-band	< 0.001	-	0.02	e^-/sec/pixel	9
H-band	< 0.001	-	0.02	e^-/sec/pixel	9
K-band	< 0.001	-	0.02	e^-/sec/pixel	9
Ghosting					
Imager	$< 10^{-5}$	-	$< 10^{-4}$	-	10
IFU	$< 10^{-5}$	-	$< 10^{-4}$	-	10

Notes:

1. Based on the area weighted rms spot diameter over the wavelength range of 0.7 to 2.40 µm.
2. Ensquared energy in a 2 x 2 pixel box centered on the image centroid over the wavelength range of 0.7 to 2.40 µm.
3. Total on-axis rms wavefront error for the imager, total rms wavefront error for the IFS optical path to the image slicer (lenslet array).
4. Total rms wavefront error at 20" radius for the imager, total rms wavefront error at 20" radius for the IFS optical path to the image slicer (lenslet array).
5. Total geometric distortion over the entire imager FOV. The intent is to limit the instrumental contribution to astrometric error to < 0.05 mas rms for the 8 mas plate scale.
6. Imager throughput, without coronagraph, QE of the science detector is not included.
7. IFS throughput, QE of the science detector is not included.
8. This is the peak variation in transmission over the full FOV.
9. This is the contribution of the instrument background to the total "dark counts"; the goal value is 10% of the goal for science detector dark current.
10. Intensity of the ghost image compared to the parent image at all wavelengths from 0.818 to 2.40 µm.

6.3 Optical Design Description

DAVINCI provides three operating modes: imager, coronagraph, and IFS. All three modes of operation are contained in a single dewar, and are fed by a single output of the second AO relay of the NGAO system. The AO relay provides a telecentric output to DAVINCI with a focal ratio of f/46. The image scale at the focal plane of the AO relay is 2.5 mm/", resulting in a 40" focal plane approximately 100 mm in diameter.

As mentioned above, it was decided that all modes of operation would share a common pupil image as a cold pupil mask or Lyot stop location, thus the first OAP relay of the instrument is shared between all modes. An optical layout of the DAVINCI instrument, including the imager light path and the integral field spectrograph scale changer, are shown in Figure 8. An annotated Zemax shaded model is shown in Figure 9 .

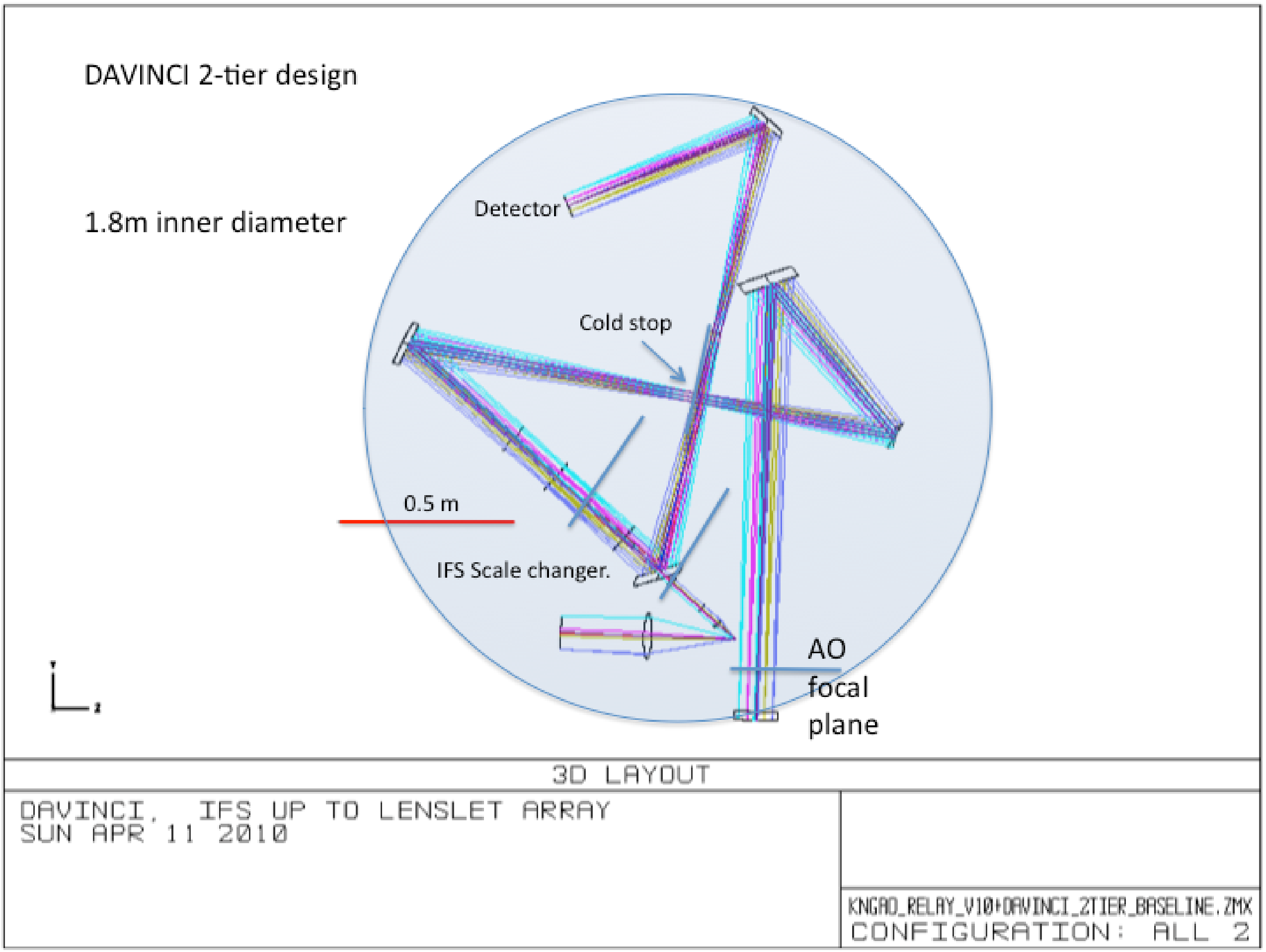

Figure 8: The DAVINCI optical layout, as seen from directly overhead

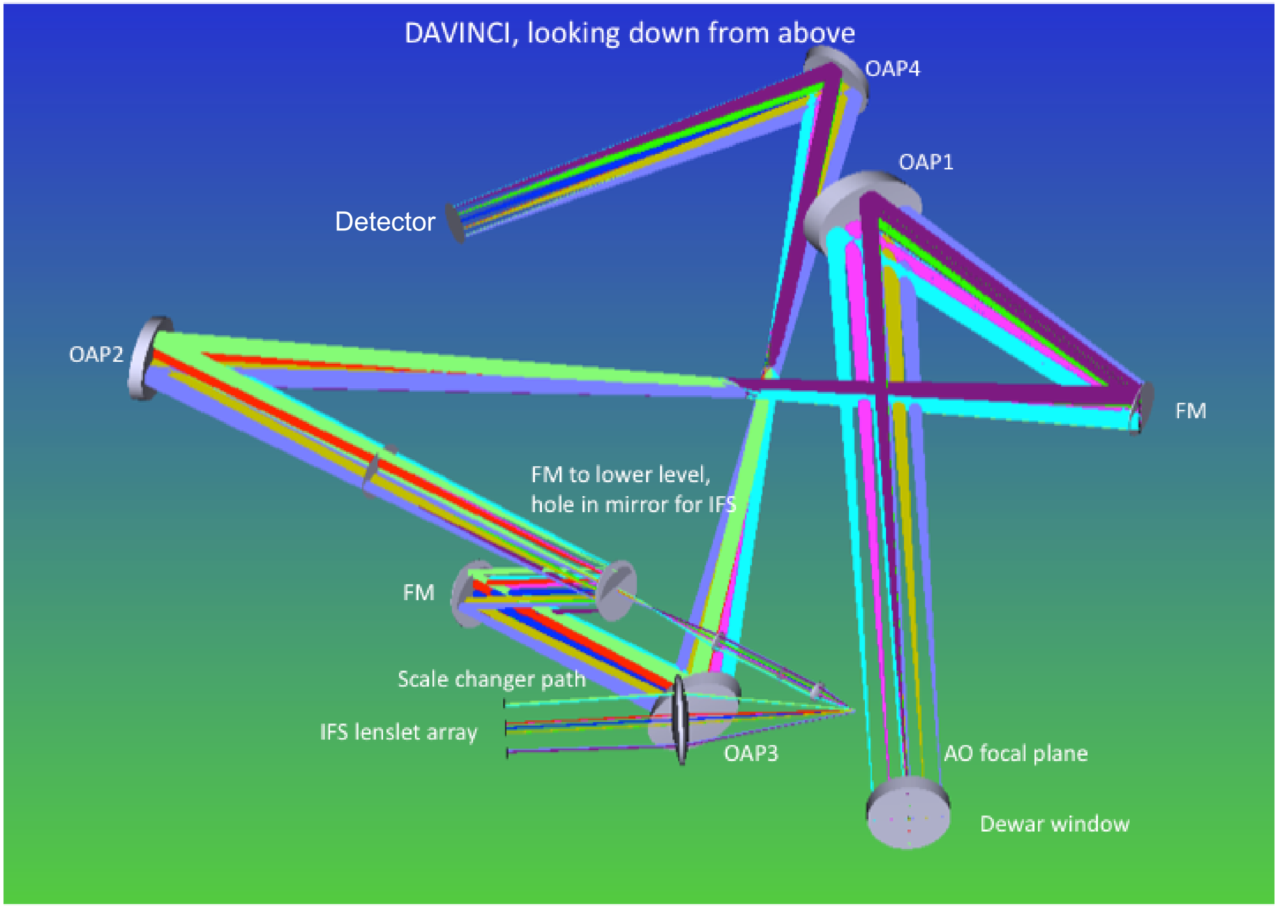

Figure 9: The DAVINCI optical layout, shown in perspective to emphasize the 2-tier design

6.3.1 Imager

The optical layout of DAVINCI's imager is illustrated in Figure 9 and Figure 10. Table 8 lists all of the optical elements in the imager with relevant dimensions. The complete optical prescription for the imager is given in appendix A.

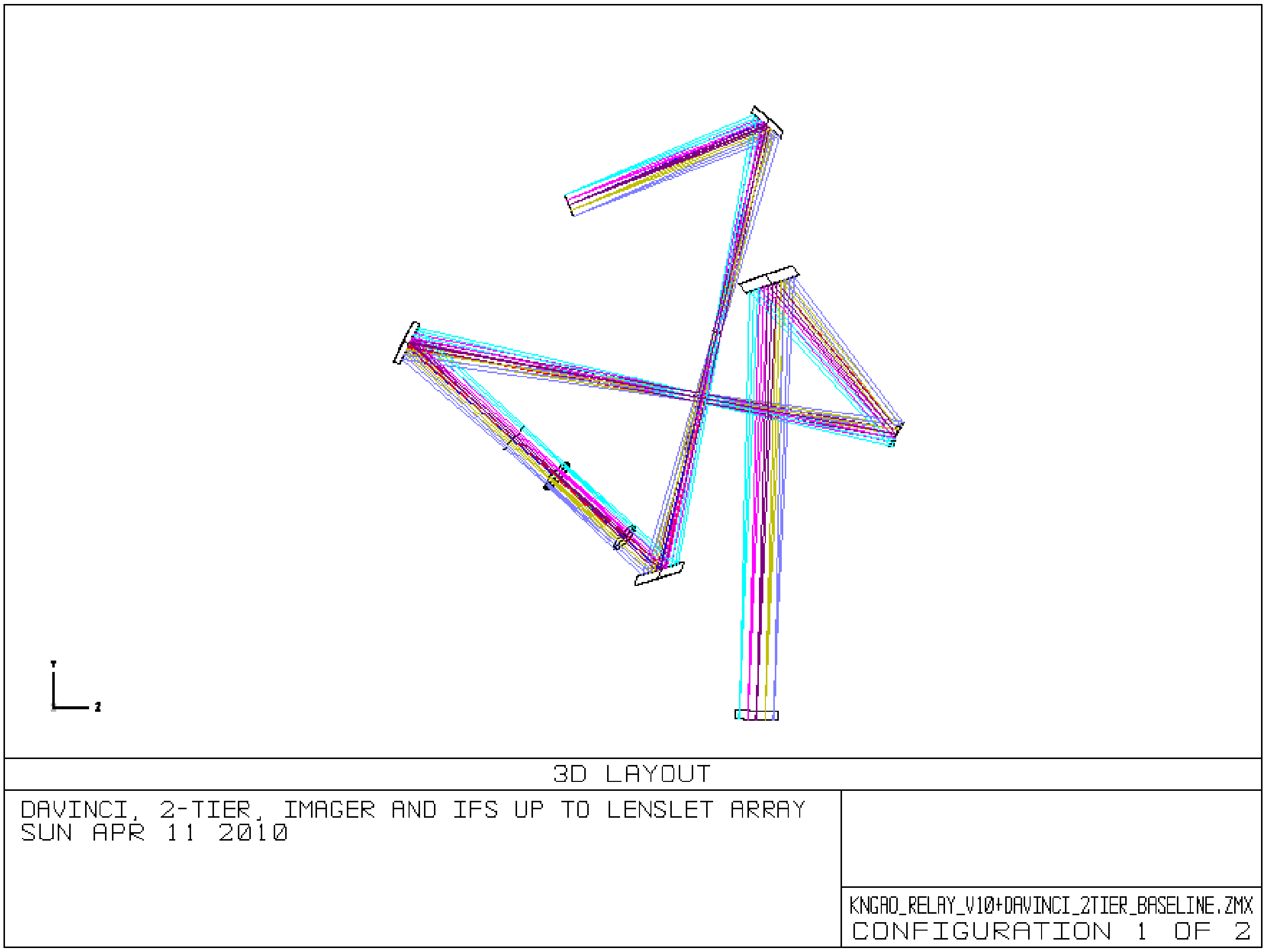

Figure 10: DAVINCI fore-optics and imager optical layout

The entrance window for the DAVINCI dewar lies in the converging beam of the AO relay's science feed, ~75mm before focus. The masks for the coronagraphic mode of the instrument are located at the AO focal plane inside the dewar.

Approximately 1 m after the focal plane is an OAP with a radius of curvature of 1998.7 mm, an off-axis angle of 41.5°, and a diameter of 150 mm. This OAP has been optimized in off-axis angle and focal length to produce a high quality, 25mm pupil image at the cold stop. This was accomplished in Zemax by producing a configuration in which the primary mirror of the telescope was the object. Geometric rays from the primary mirror "object" were used to evaluate pupil image quality after passing through both the AO relay and DAVINCI's OAP1. OAP1 compensates for some aberrations and distortions produced in the preceding AO relay. The distance between OAP1 and OAP2 is long, almost 2 m, because of the slow input f/#, the desired 25 mm pupil size at the cold stop, and the need for telecentricity on the input to the IFS. Therefore a fold mirror is located 586 mm before the cold stop for packaging.

The 40 mm diameter bandpass filters are placed following the cold stop in collimated light.

The image scale required at the detector is about 1.54 mm/", and this corresponds to an f/29 beam. Because the optics of the DAVINCI imager must provide a scale change, OAP2's focal length is shorter than OAP1's (they are not a matched pair), giving an image scale of 1.9 mm/" at the intermediate focal plane. Because this focus also acts as the feed to the integral field spectrograph, which unfortunately requires a larger focal ratio, we chose to accomplish the focal ratio reduction for the imager with both OAP relays. OAP2 has a radius of curvature of 1531.9 mm, an off-axis angle of 31.5° and a diameter of 120 mm. It is placed one focal length away from the cold stop to provide a telecentric beam to the IFS scale changer and the second relay of the imager.

To allow access to mechanisms (coronagraph mask wheel, filter wheels, pupil mask wheel, and IFS scale changer wheels) we have divided the DAVINCI imager's optical path into two tiers, with the input optical path up to the intermediate focal plane located on an upper tier, and the optical path to the imager and detector on a lower tier. Near the image plane of the first OAP relay in DAVINCI is the first of two mirrors which fold the beam down at an incidence angle of 15° to a lower level of the dewar. A matching (15°) fold mirror completes the periscope to the second level. The vertical distance between levels is 150 mm.

To complete the scale change required by the imager's detector size, a second, also unmatched, OAP relay is used. OAP3 has a radius of curvature of 1034 mm, an off-axis angle of 61.3°, and a diameter of 120 mm. It produces a collimated beam in which a pupil image is formed one focal length away from OAP3. This pupil image is not utilized, so its quality is not relevant. The final OAP in the imaging system has a radius of curvature of 962 mm, a diameter of 100 mm, and off axis angle of 54.4°. It produces an image plane ~62mm in diameter.

Table 8: Optical element specifications for the DAVINCI imager

Optic	Diameter (mm)	Radius of curvature (mm)	Off-axis angle (degrees)	Thickness (mm)
Entrance Window	120			25
OAP1	150	1998.7	41.5	
FM1	100			
OAP2	120	1531.9	31.6	
FM2	120			
FM3	90			
OAP3	120	1034	61.3	
OAP4	100	962.1	54.4	

6.3.2 IFS Scale Changer

Figure 9, Figure 11 and Figure 12 illustrate the optical design of the IFS scale changing optics. Following the first OAP pair of DAVINCI is an intermediate focal plane, at which can be placed either a fold mirror, or a fold mirror containing an aperture at its center. This aperture allows light to enter the IFS scale changer.

The integral field spectrograph is required to work at three different sampling scales. The sampling is achieved by a 1.2 mm pitch lenslet array at the focal plane of the IFS scale changer. The scale changer is required to remain a constant length, regardless of sampling scale, to keep the lenslet array and all following optics stationary. The scale changer is also required to work at wavelengths from 0.7 μm to 2.4 μm (I through K bands). To help in meeting throughput requirements it was desirable that the scale changer contain as few elements as possible.

Table 9 provides the different sampling scales, their total field size on the 80 x 80 lenslet array, their physical size at the IFS pickoff, and the magnification required. The complete optical prescription for the scale changer is given in appendix A.

Table 9: DAVINCI IFS scale changer requirements

Sampling scale (mas)	Total field size (arcseconds)	Size at IFS pickoff focal plane (mm)	Magnification required
10	0.8	1.5	64
35	2.8	5.2	18
50	4.0	6.2	13

To achieve these disparate magnifications, two relays were used, each containing two BaF2 singlets in 4f configurations. Because we also have a wide wavelength range, separate singlet pairs were designed for the visible and infrared bandpasses. The first relay contains six pairs of interchangeable lenses, mounted in wheels, relaying the image over a constant distance but with different magnifications. The second relay has a fixed magnification for all sampling scales. See Figure 12 for the optical designs of the JHK band scale changer. All six lenses of the first relay are shown in the Figure 12, top left (the first lens is very small, and close to the image plane), so that their relative positions can be seen. Figure 12, top right, shows the 10 mas relay, requiring the greatest magnification. Figure 12, bottom left is the 35 mas relay, and Figure 12, bottom right shows the relay requiring the least magnification, 50 mas. Notice that the final focal plane for all three relays is coincident and of identical size (96mm, or 80 lenslets multiplied by 1.2mm lenslet pitch). The visible band scale changer is almost identical with very slight differences in radii of curvature, image and object distances.

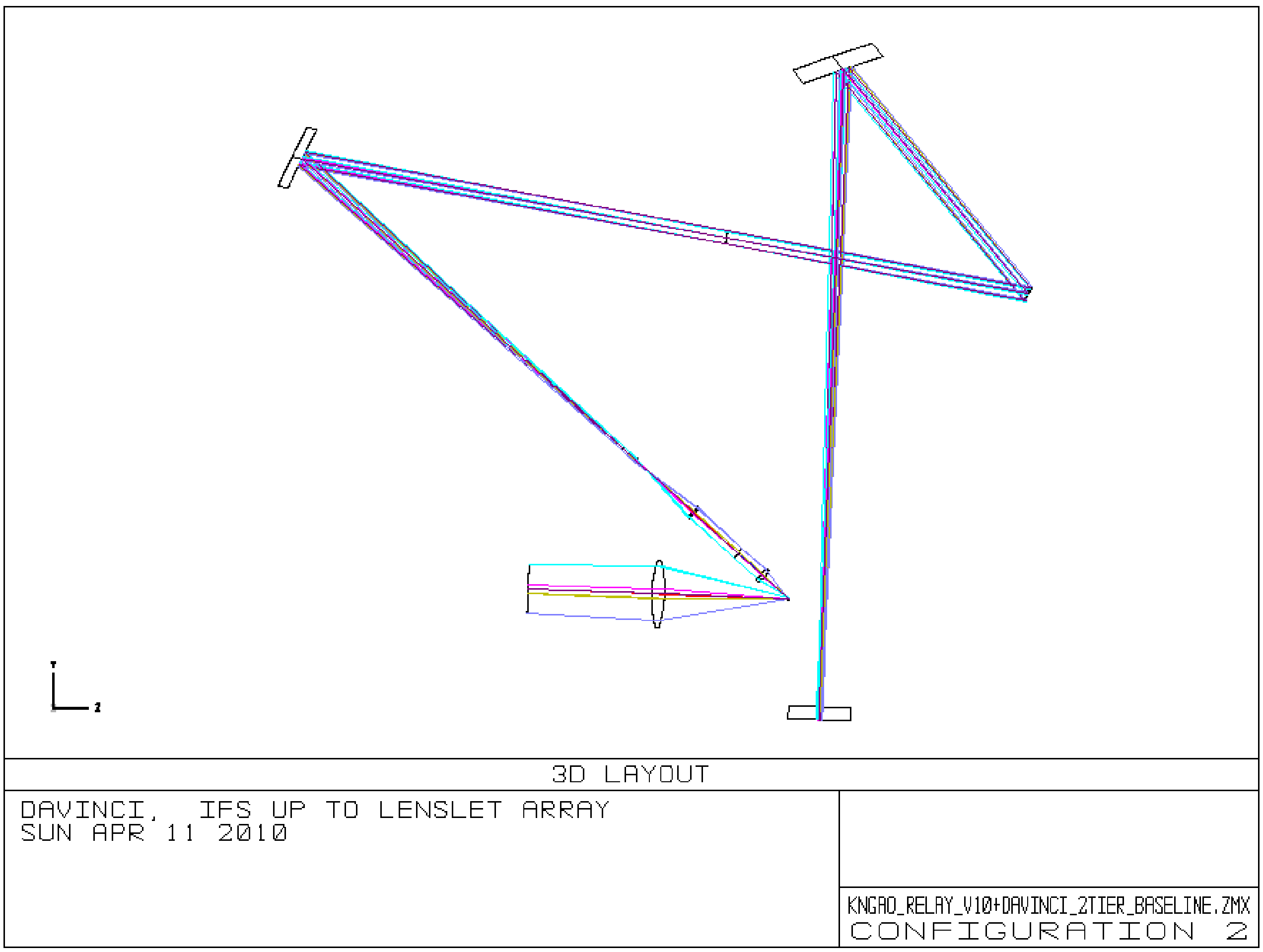

Figure 11: DAVINCI IFS fore-optics and scale changer

The scale changer contains one fold mirror between the two lenses of the fixed second relay for packaging. The total length of the scale changing optics is 930 mm. A Zemax glass file of barium fluoride tested at 120 K for MOSFIRE was included as input to the design. Unfortunately, we do not at present have index data at 120 K for wavelengths below 0.852 µm.

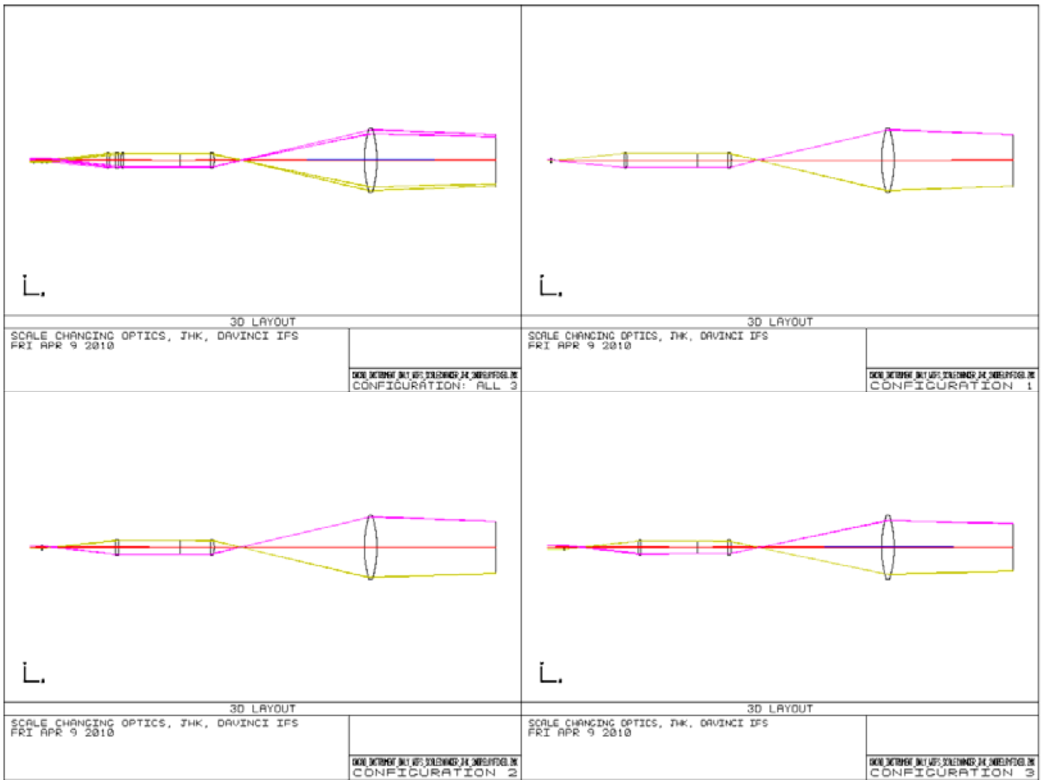

Figure 12: IFS scale changer optical layout

Clockwise from top left: All sampling scales, 10 mas, 50 mas, and 35 mas.

6.4 Design Trades

An all-refractive optical design was attempted for the DAVINCI imager, but it was found that a very large number of elements were required to reach the desired performance levels at both the pupil and image planes. This was mostly due to the large wavelength range the instrument is required to achieve. Instead, a design using all OAPs, but some with very large off-axis angle, was pursued. These off-axis angles may require special fabrication techniques, since simply cutting the OAP from a parent parabola becomes less feasible.

The spatial sampling of the integral field spectrograph will be achieved with a lenslet array having a 1.2 mm pitch to facilitate the optical design following the lenslet array. The scale changing optics would require less magnification with a smaller lenslet pitch, but the downstream optics become more cumbersome.

6.4.1 Pupil image quality

In order to maintain throughput to the detector, the pupil image at the cold stop must be of high quality. Overly aberrated pupils require undersized pupil masks, removing light from the system. The first OAP of DAVINCI was therefore designed with only the pupil image in mind. Table 10 lists the characteristics of the pupil image at the pupil mask. Figure 14 displays the results of a pupil analysis assuming the telescope mirror as the "object" and evaluating how the primary is imaged onto the cold stop plane. The geometric spots are approximately 1.6% of the size of the cold stop.

Table 10: Characteristics of the pupil image at the pupil mask

Diameter (mm)	Field considered arcseconds	Tilt, degrees	Maximum Distortion %	Geometric spot radius (µm)
25	40	57	0.23	208

Figure 13 shows the footprint of the tilted pupil at the cold stop plane. In this case, the Zemax prescription was set up normally, with field stars at infinity as the "object". Each of the differently colored rings is the pupil edge produced by a different field point at infinite conjugate. In a highly aberrated pupil, these rings would not necessarily overlap each other.

Cancelling the pupil aberrations of the preceding OAP relays introduced a large amount of tilt at the pupil plane. The pupil masks will have to be tilted to accommodate this. The pupil quality is wavelength independent because only reflective powered optics are used to produce the pupil image.

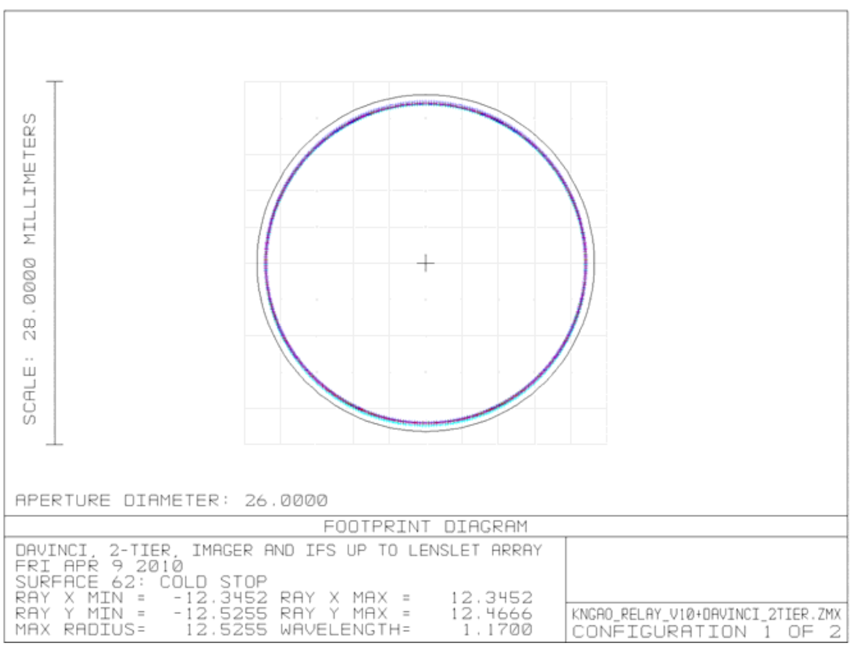

Figure 13: Pupil footprint at the tilted pupil mask

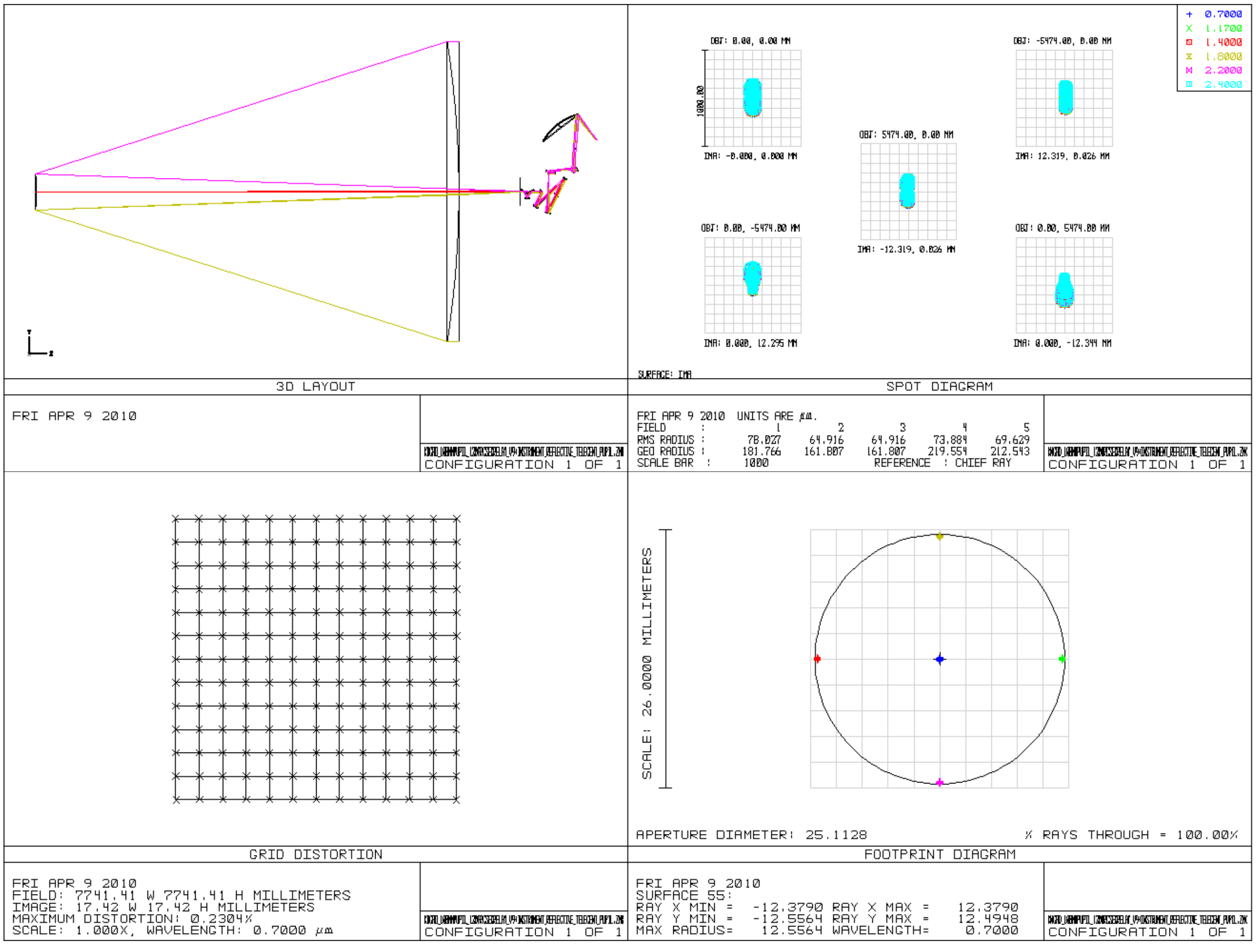

Figure 14: Characteristics of the pupil image at the pupil mask

Clockwise from top left: Zemax layout used to evaluate the pupil, geometric images of points on-axis and at edges of primary mirror(given a 40" FOV), grid distortion of the pupil image, and the footprint of the primary mirror imaged on the tilted pupil mask.

6.4.2 Image quality

The image quality of the DAVINCI imager suffers from the fact that the OAP pairs used in the instrument are not matched pairs, resulting in aberrations at extreme field points. Also, to keep distortion at acceptable levels, no attempt was made to correct field curvature at the image plane, which is the dominant source of wavefront error. On the other hand, because an entirely reflective system was designed, it suffers no color-dependent aberrations, focal shift, or lateral color. It will not require refocusing when switching to different wavelength bands. Table 11 shows the effect of adding a field flattener to the imager.

Table 11: Image quality with and without a field flattener

	FOV diameter, arcseconds	Field curvature (mm)	RMS WFE, on axis (nm)	RMS WFE, at 10 arcsecond radius (nm)	RMS WFE, at 20 arcsecond radius (nm)	Maximum grid distortion%
w/o field flattener	40	200	14	16	105	0.7
field flattener	40	0	17	9	58	5.3

A barium fluoride plano-convex singlet placed very close (~4 mm) to the focus with a radius of 75 mm on the convex surface removes the field curvature, producing diffraction-limited images at 0.7 μm across the field, but increases the maximum grid distortion to 5.3%. Smaller amounts of field curvature correction produce smaller distortion. Re-evaluating the maximum distortion requirement might be desirable to achieve diffraction-limited results at all bandpasses.

Figure 15 shows the as-built image quality without field flattening. RMS spot radii are larger than 2 pixels at the extreme field points. The system is diffraction-limited at all wavelengths for the central 20" diameter field, and diffraction-limited in K band for the entire 40" diameter field.

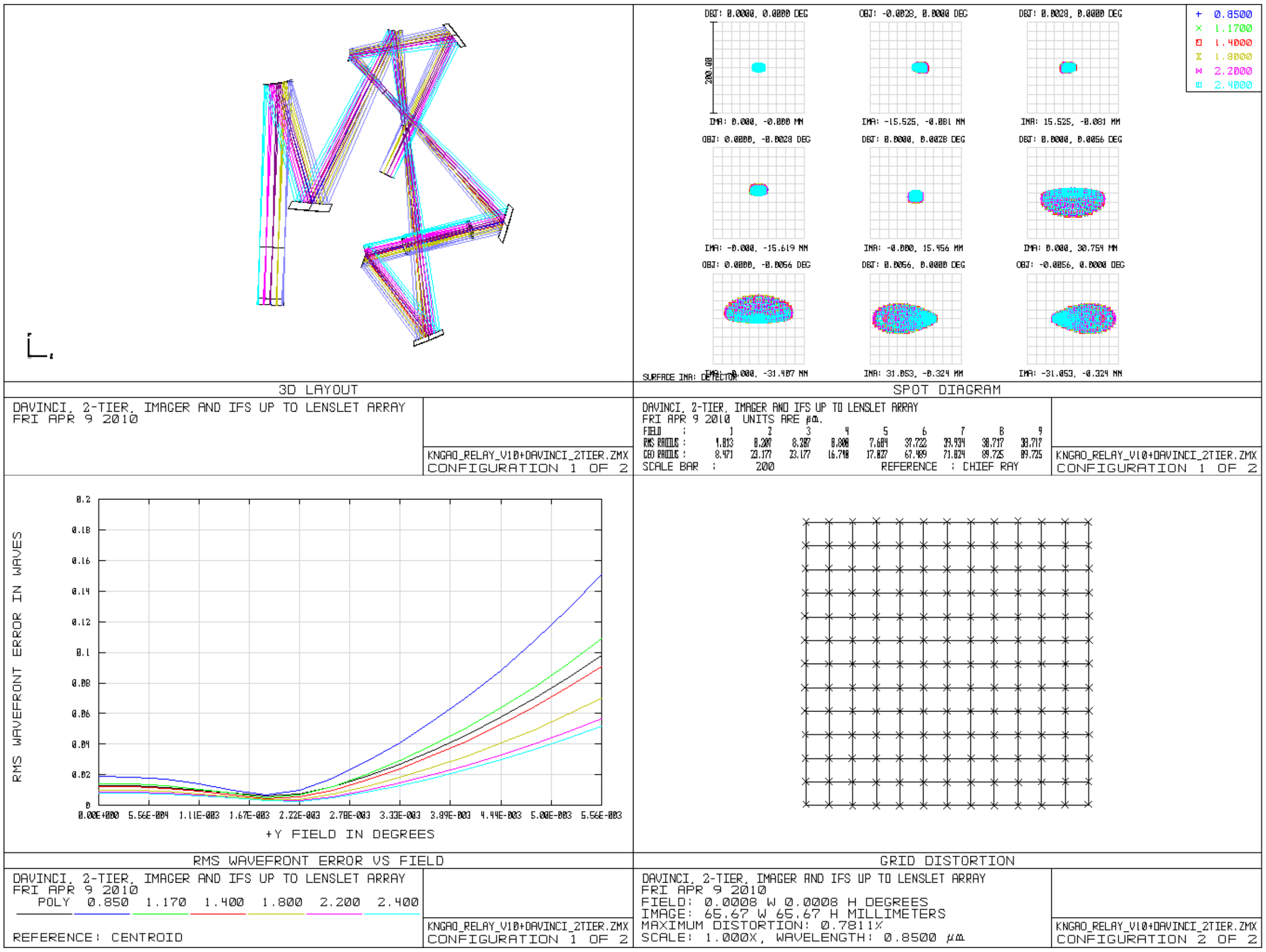

Figure 15: Image quality metrics at the DAVINCI imager's detector plane

6.4.3 Transmission

The transmissions shown in Table 12 for the DAVINCI imager were estimated using reflectance and transmittance values from the NGAO throughput and emissivity flowdown budget, version 9. It is assumed that all reflective optics are gold-coated, and all transmissive optics have a broadband AR coating

Table 12: Transmission estimates for the DAVINCI imager

Band	I	Z	J	H	K
Wavelength,μ	0.7	0.8542	1.25	1.5	2.3
Window 1	97.00%	97.00%	99.70%	99.70%	99.70%
Window 2	97.00%	97.00%	99.70%	99.70%	99.70%
OAP1	97.00%	97.00%	97.00%	97.00%	97.00%
Cold stop	100.00%	100.00%	97.00%	97.00%	97.00%
filter	90.00%	90.00%	88.00%	85.00%	95.00%
OAP2	94.59%	96.80%	98.40%	98.40%	98.70%
FM1	94.59%	96.80%	98.40%	98.40%	98.70%
OAP3	94.59%	96.80%	98.40%	98.40%	98.70%
FM2	94.59%	96.80%	98.40%	98.40%	98.70%
FM3	94.59%	96.80%	98.40%	98.40%	98.70%
OAP4	94.59%	96.80%	98.40%	98.40%	98.70%
Total	58.83%	67.58%	74.71%	72.16%	82.14%

6.4.4 Tolerances

6.4.4.1 Optical Manufacturing, Effect on Correctable and Uncorrectable WFE

An analysis of the effect of optical manufacturing errors on the total correctable and uncorrectable wavefront error has been performed for both the AO relay and the DAVINCI imager optics. Table 13 summarizes the results. Table 13 assumes manufacturing quality of $\lambda/10$ for OAPs, $\lambda/20$ for flat mirrors, and $\lambda/7$ for dichroics at the optical test wavelength of 632nm. These estimates have been obtained from optical manufacturers.

The total RMS WFE is the root sum square (RSS) of each of the elements. It is assumed that manufacturing errors follow a -2 power law in spatial frequency. The correctable wavefront error can be approximated by dividing the total RMS WFE by the square root of the number of actuators across the high order DM, in our case 64. On-axis WFE is assumed to be correctable, while the off-axis errors are not. Telescope errors, based on R. Dekany's model fit, are also included.

Table 13: Correctable and uncorrectable wavefront error due to manufacturing figure errors

Wavefront Error	# actuators	64	Test λ	6.32E-07
Correctable and Uncorrectable WFE estimates, AO Relay to Imager Detector				
λ/10 for OAPs (SORL), λ/20 for flats (Custom Scientific), λ/7 dichroics				
Static aberrations from design, WFE estimate from Zemax				40"dia. FOV
AO relay surfaces to science field	Manufacturing WFE, m	Manufacturing WfE, nm	On axis RMS WFE nm	Off axis RMS WFE, nm
AO Window 1	3.16E-08	31.6		
AO Window 2	3.16E-08	31.6		
K mirror	6.32E-08	63.2		
K mirror	6.32E-08	63.2		
K mirror	6.32E-08	63.2		
Fold	6.32E-08	63.2		
OAP1	1.26E-07	126.4		
DM1	1.26E-08	12.64		
Na dichroic science path	9.03E-08	90.28571429		
OAP2	1.26E-07	126.4		
Fold	6.32E-08	63.2		
OAP3	1.26E-07	126.4		
DM2	1.26E-08	12.64		
OAP4	1.26E-07	126.4		
IR/Vis dichroic IR path	9.03E-08	90.28571429		
DAVINCI optical path				
Window	3.16E-08	31.6		
OAP1	1.26E-07	126.4		
Fold	6.32E-08	63.2		
OAP2	1.26E-07	126.4		
Fold	6.32E-08	63.2		
Fold	6.32E-08	63.2		
OAP3	1.26E-07	126.4		
OAP4	1.26E-07	126.4		
AO relay			19.55	57.5
DAVINCI			16	105
Total (RSS) (ignoring DM print through)	4.23E-07	423.1646257	423.918038	440.4971656
total uncorrectable	5.29E-08	52.89557821	52.98975475	57.87890675
total correctable, rms		370.2690475	370.9282832	382.6182589
total correctable, PV		1282.649605	1284.933265	1325.428528
Telescope contribution, nm		79.16400043	based on R. Dekany's fit	
Total telescope + AO		430.5057948	431.2463819	447.5541217
Telescope + AO, uncorrectable		53.81322435	53.90579773	55.94426522
Telescope + AO, correctable rms		376.6925705	377.3405841	391.6098565
Telescope + AO, correctable PV		1304.901342	1307.146127	1356.576336

6.4.5 Scale changing relay for IFS

As outlined in 6.3.2, the scale changer must accommodate three different sampling scales over the wavelength range 0.7 µm to 2.4 µm. Figure 16, Figure 17, Figure 18, and Figure 19 show an analysis of the performance of the scale changing optics. Each panel contains the optical layout in top left, followed by the spot diagrams or grid distortion analyses for 10 mas sampling (top right), 35 mas sampling (bottom left), and 50 mas sampling (bottom right). The boxes in the geometric spot analyses represent the 1.2mm lenslet. Results for the entire bandpass are shown. Figure 16 and Figure 17 show the results for the optics designed to work at visible wavelengths, while Figure 18 and Figure 19 show performance for the JHK band optics.

For all sampling scales and all wavelengths, the spots remain within the 1.2mm lenslet. Distortion is only ~0.6% for all of the designs evaluated.

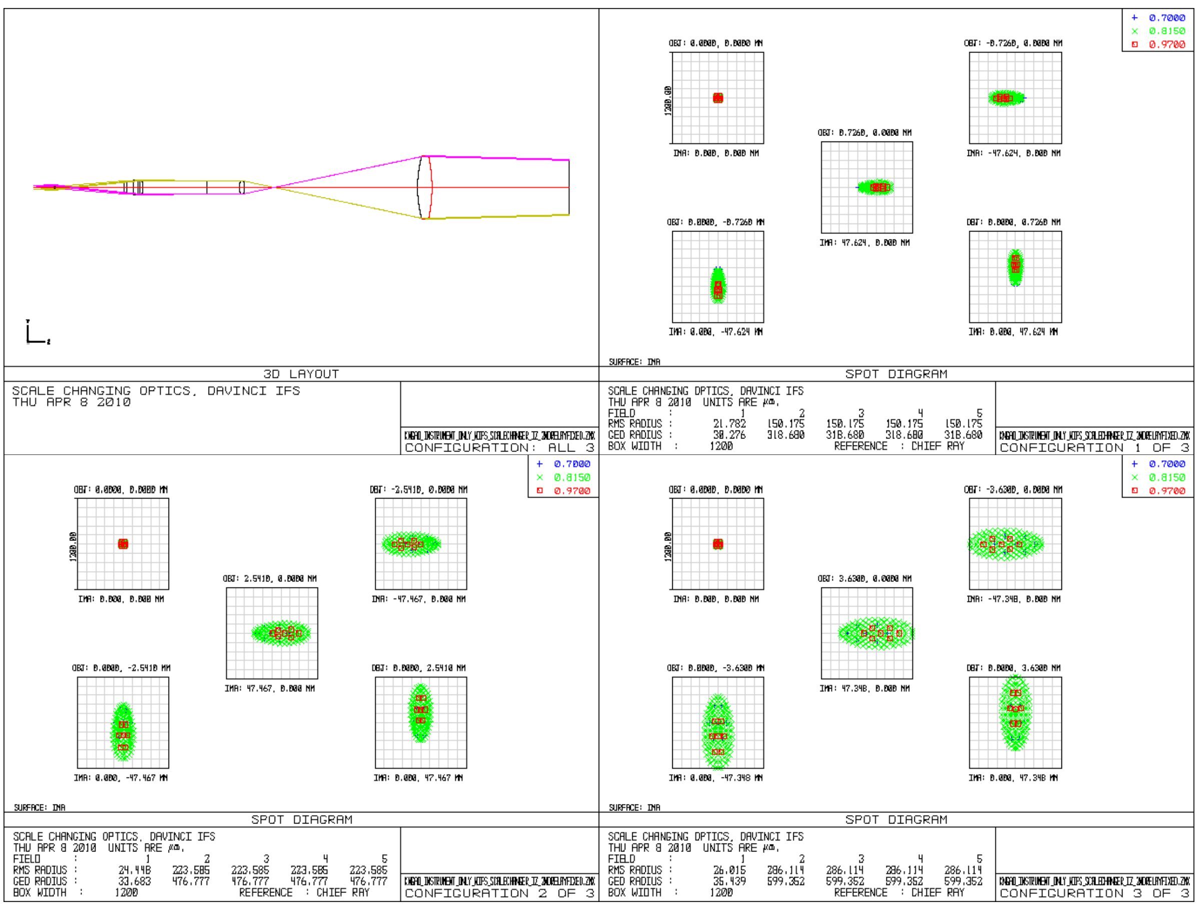

Figure 16: Geometric spot analysis of visible scale changer

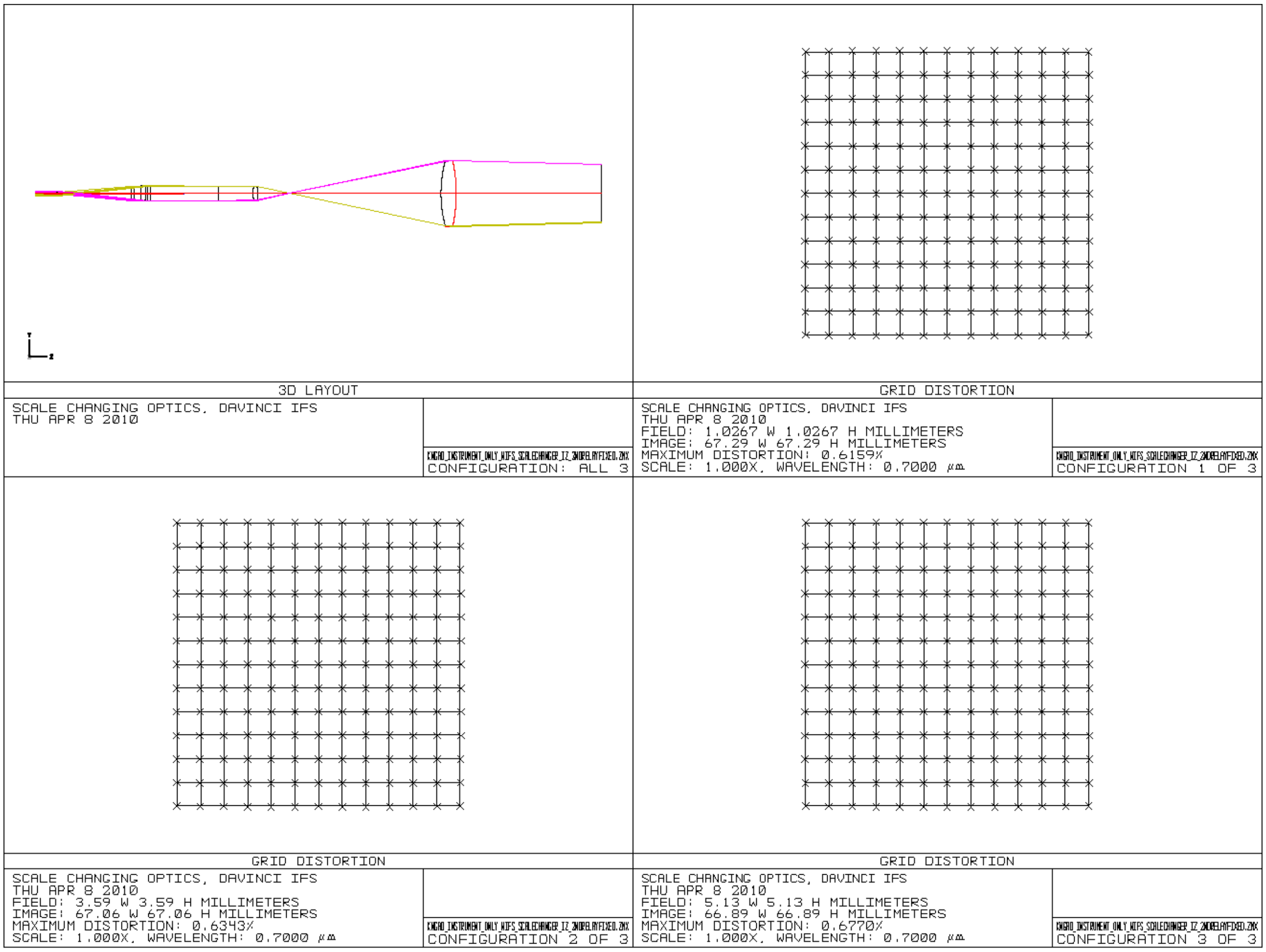

Figure 17: Grid distortion analysis for visible scale changing optics

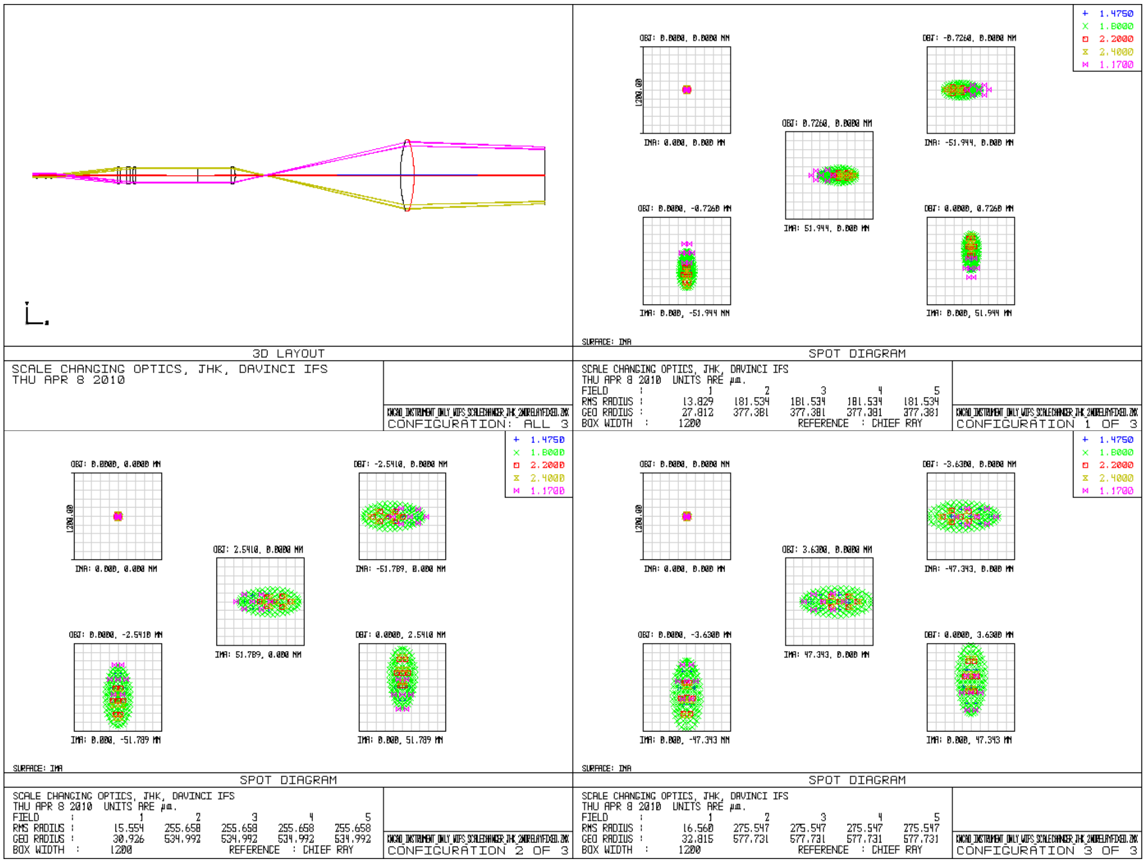

Figure 18: Geometrical spot analysis, JHK band scale changer

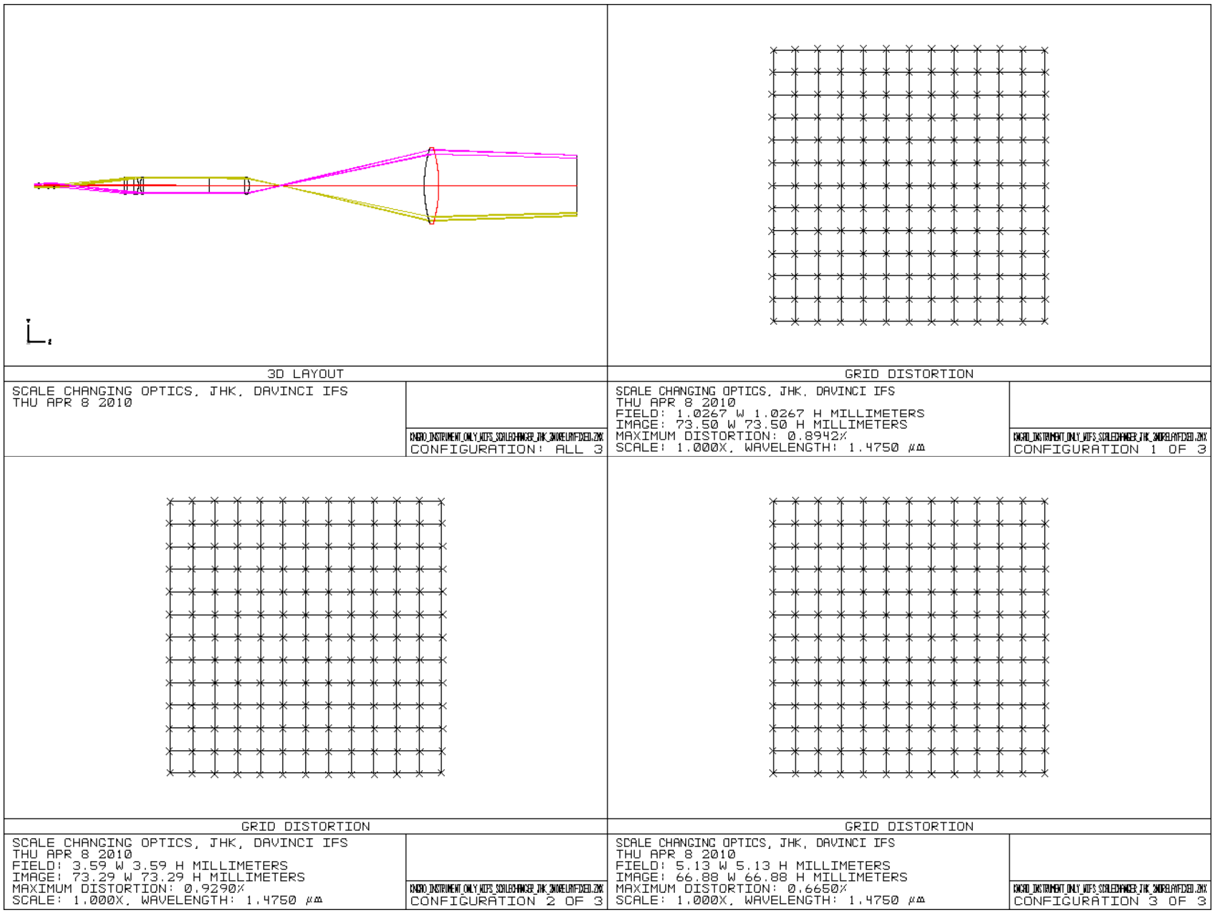

Figure 19: Grid distortion analysis, JHK-band scale changer

6.4.6 Coronagraph

DAVINCI will include a coronagraph, and our initial design is a simple Lyot coronagraph. We wanted to evaluate the performance of this approach first, but more sophisticated approaches will also be considered such as an apodized Lyot coronagraph (Soummer, 2005) or a vortex or four quadrant phase mask coronagraph. An apodizer would ideally be located exactly at a pupil plane ahead of the coronagraph mask. There is a location near a pupil plane at the second deformable mirror in the AO system, otherwise additional optics will be required to form a pupil plane for the apodizer.

6.4.6.1 Assumptions

The high contrast imaging expected performance for DAVINCI ("Keck," 2008) may be summarized as:

1. $\Delta J = 8.5$ (or contrast ratio of 4×10^{-4}) at 100 mas with a goal of $\Delta J = 11$ (4×10^{-5}) at 100 mas
2. $\Delta H = 10$ (or contrast ratio of 1×10^{-4}) at 200 mas with a goal of $\Delta H = 13$ (6.3×10^{-6}) at 1'
3. $\Delta K = 10$ (or contrast ratio of 1×10^{-4}) at 100 mas

The FOV considered for coronagraphy is only 1" therefore the field aberrations – and the pupil distortions – are negligible. We did consider a hexagonal pupil, although the shape of the aperture is not the limiting factor in the final performance.

Simulations have been done using an f/46 input beam and a Lyot stop of 25mm. We studied the performance in three observing bands, J (1.2 µm), H (1.6 µm) and K (2 µm).

Median seeing for Keck is assumed to be 0.8" and the effect of the turbulence is corrected using a square region of 62 x 62 actuators in a MEMS deformable mirror (DM). Assuming an rms wavefront error of 170 nm, the Strehl performance of the AO system for this application depends on the wavelength and is: K: 75%-82%, H: 60%, J: 40%-56%, I: 10%-22% (Dekany et al., 2009).

In theory and without aberrations, the optimum focal plane mask (FPM) depends on the wavelength, the shorter the wavelength, the smaller the FPM. However, the Strehl ratio decreases with wavelength, meaning that the halo fraction will increase leading to the need for a bigger FPM than for the perfect case. This is expected to reduce the number of different sized FPMs needed in practice.

6.4.6.2 Simulation Results

The performance of a simple Lyot coronagraph was simulated using an IDL program. The code is based on the fact that focal planes and pupil planes are related by a Fourier Transform.

The simulation is based on an f/46 beam converging onto the focal plane mask at each wavelength. The sampling resolution of the diffraction limited spot in the simulation is arbitrarily set to 12 simulation pixels per FWHM (defined as f# x λ). The pixel size in the focal plane is thus (f# x λ)/12.

The FPM is either an opaque dot or a 10% transmission dot to be able to eliminate most of the light coming from the parent star but still see the star for astrometry and photometry (some precise calibration will be needed). Such technique is being used on NICI (Chun et al., 2008).

The energy distribution in the following pupil plane or Lyot plane is the Fourier transform to get to the Lyot plane where we put an aperture to block the diffracted light from the FPM.

By the definition of the Fourier Transform, the pixel size on the pupil plane is equal to (λ x f1)/(n x θpixel), where f1 is the focal length of the first lens and θpixel the pixel size in the focal plane. We chose f1 from the f# and the diameter of the pupil in the Lyot plane (f1 = f# x d).

As stated earlier, the aberrations of the wavefront in the pupil plane are negligible because the FOV of that particular mode is very small (only 1"). Our initial simulations consider the effects of AO correction with a first approximation that considers only fitting error, using a high pass filter with a cut-off frequency set by the number of actuators. Another more accurate technique is to consider a parabolic filter instead of a Heaviside function (Sivaramakrishnan et al., 2001). The most precise estimation of the performance would be obtained by simulating true point spread functions after correction with the Keck NGAO. More thorough simulations including Strehl will be done to determine if the results found here will hold with less optimum corrections. Indeed, the Strehl in these initial simulations was kept relatively high (around 80%) which is a good approximation for K band but not for J band. We also will consider the effects of a 90% opaque FPM to account for astrometry and photometry

6.4.6.3 Results

Performance was estimated by determining the contrast obtained as a function of separation. The separation is given both in arcseconds and in cycles per aperture where one cycle per aperture is defined by the pitch of one actuator on the second DM in the AO relay.

Naturally, the results depend on the wavelength both because of the size of the spot at the focal plane and the AO correction obtained. They also depend on the size of the FPM and the size of the

Lyot stop. We therefore studied contrast curves as a function of Lyot mask and FPM sizes. The goal is to define the best combination (Lyot, FPM) as a function of wavelength.

The FPM size d was varied from 2 to 12 λ/d. For the Lyot stop, only sizes bigger than 60% of the full aperture were considered because for smaller apertures, the transmitted flux goes down significantly.

The following graphs show the resulting contrast curves for the best combinations (Lyot mask, FPM), for the three different bands. A common solution was sought for the three bands in order to minimize the number of masks needed. In the following, the FPM sizes are given in λ/d. For the 3 wavelength chosen, there is a factor of 1.6 and 1.3 respectively between J and K, and between J and H. To reach the 100 mas inner working angle, an FPM equal or smaller than 5 λ/d is required for K band, 6 λ/d in H and 8λ/d in J. The Lyot mask remains the same size in all three bands. A reduction of the Lyot mask size from 90% to 75%, causes a decrease in sensitivity of 2.5 x Log(0.833^2) or 0.4 magnitudes.

6.4.6.3.1 J Band

For J band the Strehl is overestimated using the simple method of a Heaviside high pass filter. The requirements ask for an inner working angle smaller than 100 mas. The diffraction-limited spot is 25 mas and the maximum FPM size is thus 8λ/d diameter at 1.2 μm. For this band we varied the FPM radius from 3 to 8 λ/d by increments of 1 λ/d and the Lyot size from 75 to 90% by increments of 2.5%.

The best combination using the biggest size Lyot stop is (82.5%, 8), which is at the limit of the required separation (Figure 20). To increase the inner working angle and optimize the same FPM for a different wavelength, we need to reduce the size of the Lyot mask to 75% and use an FPM of diameter equal to 5λ/d (Figure 21). This reduces the transmission, but in this exercise the goal is to optimize the inner working angle instead of the flux. One could consider increasing the FPM to increase the Lyot stop mask and therefore increase the flux.

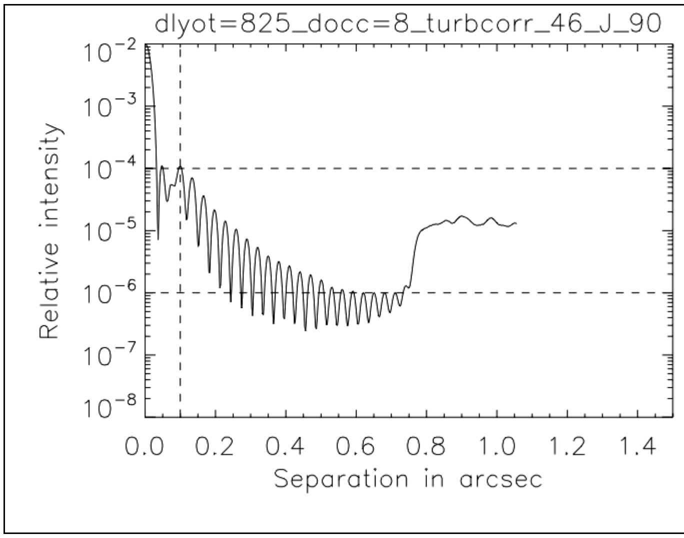

Figure 20: J band contrast (82.5%, 8) case

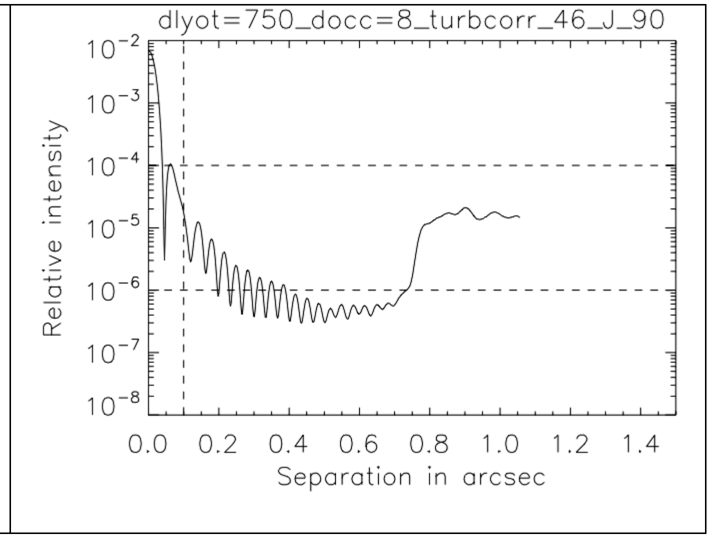

Figure 21: J band contrast (75%, 5) case

The plateau at about 0.8" is due to the limit at which the DM can control and correct the wavefront.

6.4.6.3.2 H Band

The requirements ask for an inner working angle of 200 mas. The diffraction-limited spot is equal to 33 mas and the maximum FPM size is thus 12λ/d radius at 1.6 µm. For this band we varied the FPM radius from 3 to 12 λ/d by increments of 1 λ/d and the Lyot size from 75 to 90% by increments of 2.5%.

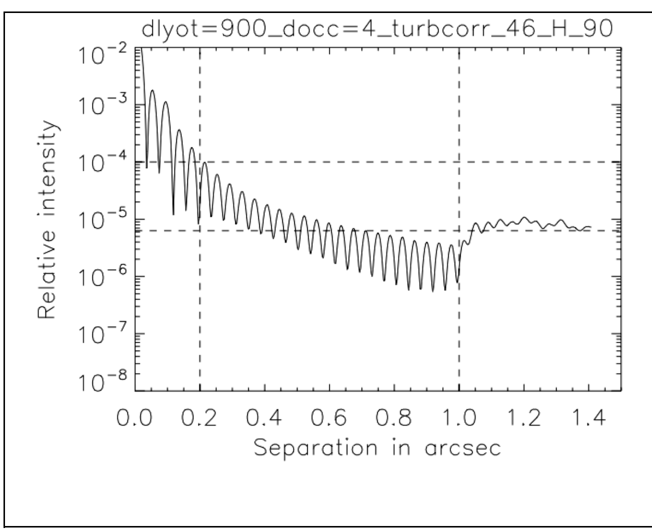

Figure 22: H band (90%, 4) case

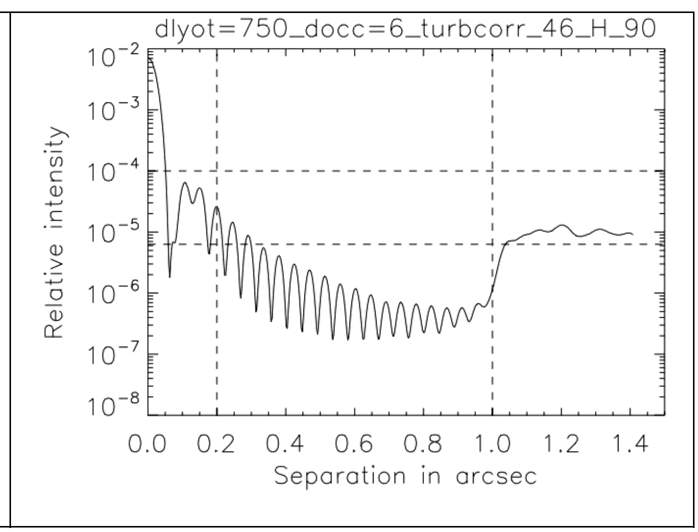

Figure 23: H band (75%, 6) case

The best combination is (90%, 4) to meet the requirements both at 200 mas and 1' (Figure 22). To minimize the changes in FPM sizes and Lyot stops between different wavelengths so far (J and H), one would have to choose the combination (75%, 6) as shown in Figure 23. The resulting contrast is even better at this wavelength.

6.4.6.3.3 K Band

The requirements ask for an inner working angle of 100 mas. The diffraction-limited spot is equal to 41 mas and the maximum FPM size is thus 5λ/d diameter at 2 μm. For this band we varied the FPM radius from 2 to 5 λ/d in increments of 1 λ/d and the Lyot size from 75 to 90% by increments of 2.5%. Because of previous results, we increased the range of the FPM size to 6λ/d.

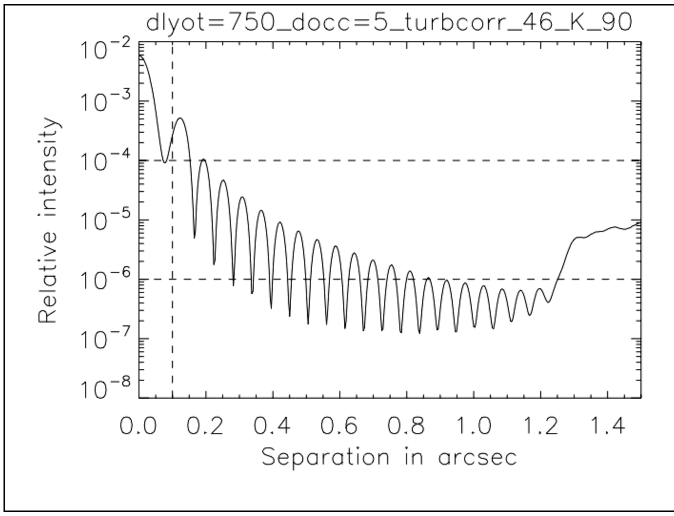

Figure 24: K band (75%, 5) case

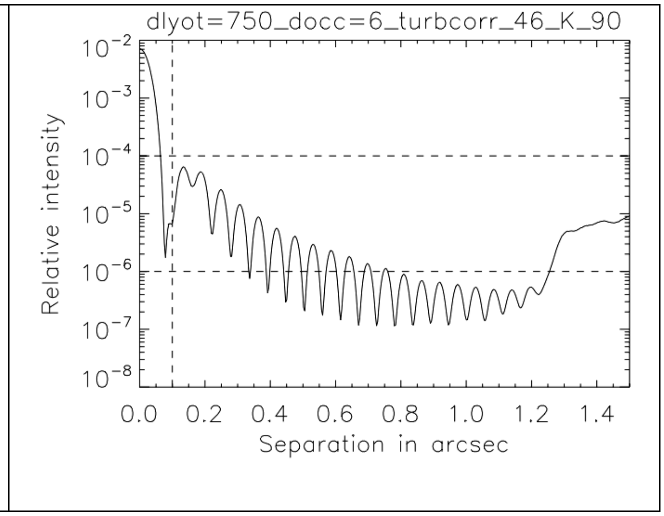

Figure 25: K band (75%, 6) case

To keep an inner working angle of 100 mas without loosing too much light, the best combination is (75%, 5) as seen in Figure 24. However, the contrast at 100 mas is higher than 10^{-4}. The combination (75%, 6) leads to better performance for a slightly bigger inner working angle (Figure 25).

6.4.6.4 Sensitivity

The SNR vs. exposure time for companions of K band magnitudes of 18 and 24 are shown in Figure 26 for the (75%, 6) and (100%, 6) cases.

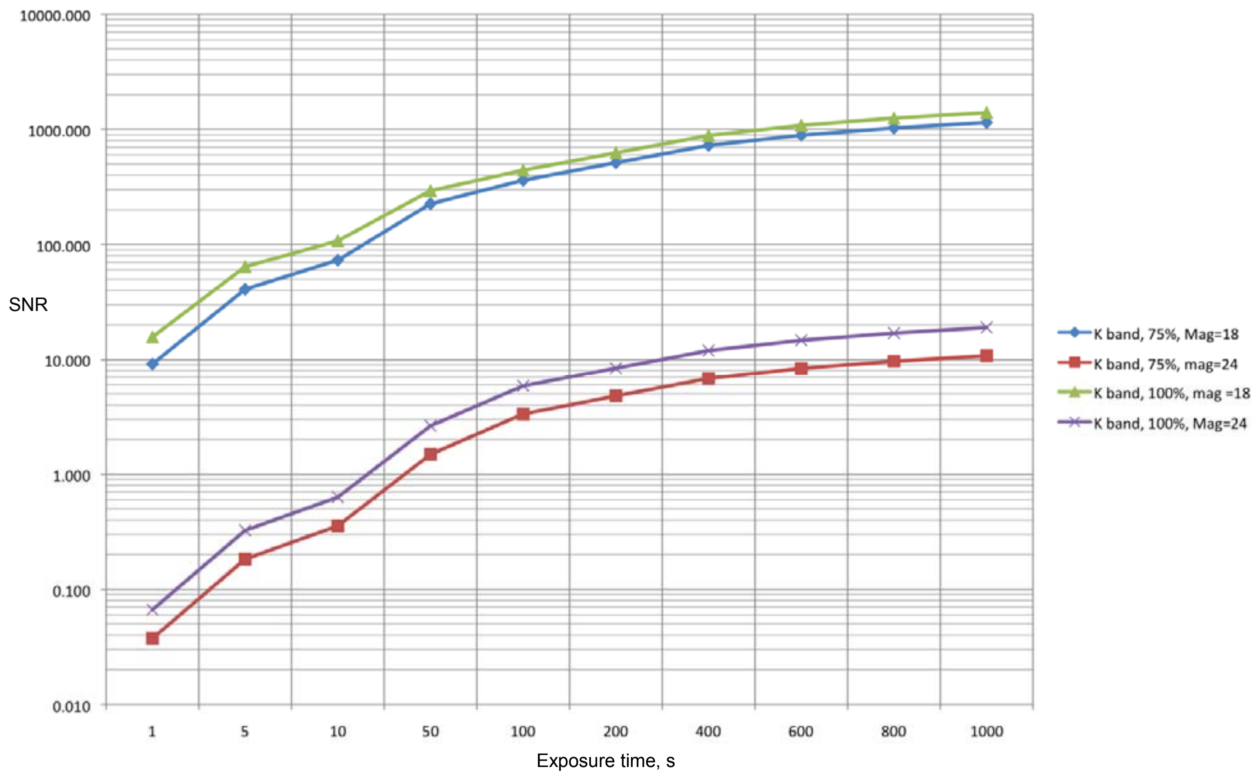

Figure 26: DAVINCI coronagraph companion sensitivity in K band

6.4.6.5 Conclusions

A simple Lyot coronagraph meets our requirements if the transmission losses and some compromises of inner working angles are acceptable. The best common combination is to use a Lyot mask of 75% the nominal pupil size and a focal plane mask of 100 mas. In order to further improve performance, we will need to use an apodizer, or consider other techniques such as a vortex coronagraph or quadrant phase masks.

7 REFERENCES

Adkins, S. (2009, January 20). Keck Next Generation Adaptive Optics Detectors for NGAO Instrumentation. Keck Adaptive Optics Note 556. Waimea, HI: W. M. Keck Observatory.

Baek, M. & Marchis, F. (2007, November 27). Next Generation Adaptive Optics: Optimum Pixel Sampling for Asteroid Companion Studies. Keck Adaptive Optics Note 529. Waimea, HI: W. M. Keck Observatory.

Beck, T.L., McGregor, P. J., Takami, M. & Pyo, T. (2008). Spatially resolved molecular hydrogen emission in the inner 200 AU environments of classical T Tauri stars. *The Astrophysical Journal, 676* (1), 472-489.

Britton, M., Dekany, R., Flicker, R., Max, C., Neyman, C. & Olsen, K. (2007, April 10). AO Photometry for NGAO. Keck Adaptive Optics Note 474. Waimea, HI: W. M. Keck Observatory.

Cameron, B., Britton, M., Lu, J., Ghez, A., Dekany, R., Max, C. & Neyman, C. (2007, May 3). Astrometry for NGAO. Keck Adaptive Optics Note 480. Waimea, HI: W. M. Keck Observatory.

Chun, M., Toomey, D., Wahhaj, Z., Biller, B., Artigau, E., Hayward, T., Liu, M., Close, L., Hartung, M., Rigaut, F., & Ftaclas, C. (2008). Performance of the near-infrared coronagraphic imager on Gemini-South. *Proceedings of the SPIE, 7015*, 70151V1-70151V9.

Dekany, R., Neyman, C., Wizinowich, P., McGrath, E. & Max, C. (2009, March 10). Build-to-Cost Architecture Wavefront Error Performance. Keck Adaptive Optics Note 644. Waimea, HI: W. M. Keck Observatory.

Hardy, J. W. (1998). *Adaptive optics for astronomical telescopes*. Oxford, UK: Oxford University Press.

Keck Next Generation Adaptive Optics Science Case Requirements Document. (2009, January 27). Keck Adaptive Optics Note 455 [Release 2.2_v6]. Waimea, HI: W. M. Keck Observatory.

Kulas, K. (2010, January). MOSFIRE detector testing status. Retrieved January 15, 2010 from http://irlab.astro.ucla.edu/mosfire/team/meetings/meeting63/20100115-MOSFIRE%20Detector-Kulas.ppt

Kupke, R. (2009, June 11). Keck NGAO Relay Design.

Larkin, J., Barczys, M., Krabbe, A., Adkins, S., Aliado, T., Amico, P., Brims, G., Campbell, R., Canfield, J., Gasaway, T., Honey, A., Iserlohe, C., Johnson, C., Kress, E., LaFreniere, D., Lyke, J., Magnone, K., Magnone, N., McElwain, M., Moon, J., Quirrenbach, A., Skulason, G., Song, I., Spencer, M, Weiss, J., Wright, S. (2006). OSIRIS: a diffraction limited integral field spectrograph for Keck. *New Astronomy Reviews 50*(4-5), 362-364.

McLean, I. S., Steidel, C. C., Matthews, K., Epps, H., & Adkins, S. M. (2008). MOSFIRE: A multi-object near-infrared spectrograph for the Keck Observatory. *Proc. SPIE 7014*, 70142Z-70142Z-12.

MOSFIRE: Multi-Object Spectrograph for Infra-Red Exploration, detailed design report. (2007, April 6). http://irlab.astro.ucla.edu/mosfire/MOSFIRE%20DDR%20Report%20v2.pdf

Roth, M. M. (2006). PSF-fitting techniques for crowded field 3D spectroscopy. *New Astronomy Reviews, 49*, 573-581.

Sivaramakrishnan, A., Koresko, C. D., Makidon, R. B., Berkefeld, T., & Kuchner, M. J. (2001). Ground-based coronagraphy with high-order adaptive optics. *The Astrophysical Journal, 552*(1), 397-408.

Soummer, R. (2005). Apodized pupil Lyot coronagraphs for arbitrary telescope apertures. *The Astrophysical Journal, 618*(2), L161-L164.

8 APPENDIX A – ZEMAX PRESCRIPTION

8.1 DAVINCI Imager Zemax Prescription

System/Prescription Data

File:
\\.psf\Home\Desktop\Keck\designs\preliminary_design_phase\KNGAO_relay_v10+davinci_2tier_baseline.ZMX

Title: DAVINCI, 2-tier, Imager and IFS up to Lenslet array
Date : MON APR 12 2010
Configuration 1 of 2

GENERAL LENS DATA:

Surfaces : 94
Stop : 1
System Aperture : Entrance Pupil Diameter = 10949
Glass Catalogs : INFRARED MISC HERAEUS MOSFIRE
Ray Aiming : Real Reference, Cache On
X Pupil shift : 0
Y Pupil shift : 0
Z Pupil shift : 0
X Pupil compress : 0
Y Pupil compress : 0
Apodization : Uniform, factor = 0.00000E+000
Temperature (C) : 2.00000E+001
Pressure (ATM) : 1.00000E+000
Adjust Index Data To Environment : Off
Effective Focal Length : -172898.3 (in air at system temperature and pressure)
Effective Focal Length : -172898.3 (in image space)
Back Focal Length : -39.11141
Total Track : 20587.38
Image Space F/# : 15.79124
Paraxial Working F/# : 15.79124
Working F/# : 29.25044
Image Space NA : 0.03164726
Object Space NA : 5.4745e-007
Stop Radius : 5474.5
Paraxial Image Height : 12.81287
Paraxial Magnification : 0
Entrance Pupil Diameter : 10949
Entrance Pupil Position : 0
Exit Pupil Diameter : 8226.908

Exit Pupil Position : 240793
Field Type : Angle in degrees
Maximum Radial Field : 0.005556
Primary Wavelength : 1.17 μm
Lens Units : Millimeters
Angular Magnification : 1042.323

Fields : 9
Field Type: Angle in degrees

#	X-Value	Y-Value	Weight
1	0.000000	0.000000	100.000000
2	-0.002778	0.000000	3.000000
3	0.002778	0.000000	3.000000
4	0.000000	-0.002778	3.000000
5	0.000000	0.002778	3.000000
6	0.000000	0.005556	3.000000
7	0.000000	-0.005556	3.000000
8	0.005556	0.000000	3.000000
9	-0.005556	0.000000	3.000000

Vignetting Factors

#	VDX	VDY	VCX	VCY	VAN
1	0.000000	0.000000	0.000000	0.000000	0.000000
2	0.000000	0.000000	0.000000	0.000000	0.000000
3	0.000000	0.000000	0.000000	0.000000	0.000000
4	0.000000	0.000000	0.000000	0.000000	0.000000
5	0.000000	0.000000	0.000000	0.000000	0.000000
6	0.000000	0.000000	0.000000	0.000000	0.000000
7	0.000000	0.000000	0.000000	0.000000	0.000000
8	0.000000	0.000000	0.000000	0.000000	0.000000
9	0.000000	0.000000	0.000000	0.000000	0.000000

Wavelengths : 6
Units: μm

#	Value	Weight
1	1.170000	1.000000
2	1.400000	1.000000
3	1.800000	1.000000
4	2.200000	1.000000
5	2.400000	0.500000
6	0.852000	1.000000

SURFACE DATA SUMMARY:

Surf	Type	Radius	Thickness	Glass	Diameter	Conic	Comment
OBJ	STANDARD	Infinity	Infinity		0	0	
STO	STANDARD	-34974	-15394.99	MIRROR	10949	-1.003683	Keck Primary
2	STANDARD	-4737.916	15394.99	MIRROR	1317.129	-1.644326	Keck Secondary
3	STANDARD	Infinity	2227		208.4837	0	
4	STANDARD	Infinity	272.6466		1000	0	Bulkhead
5	STANDARD	Infinity	-121		29.01261	0	
6	COORDBRK	-	0		-	-	K-mirror rotation
7	STANDARD	Infinity	-243.5	MIRROR	80.38487	0	K mirror 1
8	STANDARD	Infinity	243.5	MIRROR	45.03469	0	K mirror 2
9	STANDARD	Infinity	-150	MIRROR	120.4903	0	K mirror 3
10	STANDARD	Infinity	-247.5		67.5545	0	
11	COORDBRK	-	0		-	-	
12	STANDARD	Infinity	0	MIRROR	107.1503	0	
13	COORDBRK	-	0		-	-	
14	COORDBRK	-	-763.5		-	-	derotate, go 2 focus
15	COORDBRK	-	1276.746		-	-	start 100mm relay
16	STANDARD	-2553.493	0	MIRROR	1261.576	-1	oap1
17	COORDBRK	-	-1492.194		-	-	
18	COORDBRK	-	0		-	-	
19	SZERNSAG	Infinity	0	MIRROR	100.4568	0	100 mm pupil
20	COORDBRK	-	0		-	-	
21	STANDARD	Infinity	625		99.11726	0	
22	COORDBRK	-	0		-	-	start LGS dich
23	STANDARD	Infinity	20	SILICA	190	0	LGS dichroic
24	STANDARD	Infinity	0		190	0	
25	COORDBRK	-	0		-	-	end LGS dich
26	STANDARD	Infinity	-645		111.9833	0	
27	COORDBRK	-	1408.95		-	-	
28	STANDARD	-2553.493	0	MIRROR	1258.904	-1	oap2
29	COORDBRK	-	-500		-	-	
30	STANDARD	Infinity	-908.7574		96.09241	0	relay 1, end
31	STANDARD	Infinity	-100		29.15745	0	intermediate focus
32	COORDBRK	-	0		-	-	
33	STANDARD	Infinity	0	MIRROR	53.41566	0	fold to second relay
34	COORDBRK	-	-100		-	-	
35	COORDBRK	-	317.9877		-	-	
36	STANDARD	-635.9754	0	MIRROR	197.37	-1	OAP 3
37	COORDBRK	-	-326.2408		-	-	
38	COORDBRK	-	0		-	-	
39	SZERNSAG	Infinity	0	MIRROR	24.42455	0	tweeter
40	COORDBRK	-	0		-	-	

41	COORDBRK	-	1234.04		-	-	
42	STANDARD	-1907.925	0	MIRROR	1581.917	-1	OAP4
43	COORDBRK	-	-350		-	-	
44	COORDBRK	-	0		-	-	
45	STANDARD	Infinity	0	MIRROR	127.9385	0	switchyard
46	COORDBRK	-	400		-	-	
47	STANDARD	Infinity	437		110.2178	0	
48	STANDARD	Infinity	25	INFRASIL	120	0	dewar window
49	STANDARD	Infinity	78.556		120	0	
50	COORDBRK	-	999.3693		-	-	
51	STANDARD	-1998.737	0	MIRROR	1634.063	-1	oap1_instr
52	COORDBRK	-	-700		-	-	
53	COORDBRK	-	0		-	-	
54	STANDARD	Infinity	0	MIRROR	80.80314	0	
55	COORDBRK	-	0		-	-	
56	STANDARD	Infinity	586.4909		75.23125	0	
57	STANDARD	Infinity	0		26.59406	0	cold stop
58	STANDARD	Infinity	888.292		26.59406	0	
59	COORDBRK	-	0		-	-	
60	STANDARD	-1531.855	0	MIRROR	961.4958	-1	oap2_instr
61	COORDBRK	-	-474.9427		-	-	
62	STANDARD	Infinity	-423.5805		85.66672	0	
63	STANDARD	Infinity	0		74.75814	0	ifs pickoff
64	COORDBRK	-	0		-	-	
65	STANDARD	Infinity	0	MIRROR	90	0	fold up to 2nd tier
66	COORDBRK	-	300		-	-	
67	COORDBRK	-	0		-	-	
68	STANDARD	Infinity	0	MIRROR	100	0	periscope
69	COORDBRK	-	0		-	-	
70	STANDARD	Infinity	300		83.09185	0	
71	COORDBRK	-	-516.5		-	-	
72	STANDARD	1034.001	0	MIRROR	1317.671	-1	oap3_instr
73	COORDBRK	-	879.1171		-	-	
74	STANDARD	Infinity	0		25.84208	0	
75	STANDARD	Infinity	735.41		25.84208	0	
76	COORDBRK	-	0		-	-	
77	STANDARD	-962.1413	0	MIRROR	1074.076	-1	oap4_instr
78	COORDBRK	-	-828		-	-	
IMA	STANDARD	Infinity			62.80239	0	detector

8.2 JHK Scale Changer

System/Prescription Data

File:
\\.psf\Home\Documents\Dropbox\KNGAO_instrument_only_wifs_scalechanger_jhk_2ndrelayfixed.ZMX

Title: Scale changing optics, JHK, DAVINCI IFS
Date : MON APR 12 2010
Configuration 1 of 3

LENS NOTES:
config 1 800
config 2 801
config 3 802

GENERAL LENS DATA:

Surfaces : 12
Stop : 1
System Aperture : Object Space NA = 0.01489
Telecentric Object Space: On
Glass Catalogs : MISC SCHOTT HERAEUS OHARA INFRARED MOSFIRE
Ray Aiming : Off
Apodization : Uniform, factor = 0.00000E+000
Temperature (C) : 2.00000E+001
Pressure (ATM) : 1.00000E+000
Adjust Index Data To Environment : Off
Effective Focal Length : 1e+010 (in air at system temperature and pressure)
Effective Focal Length : 1e+010 (in image space)
Back Focal Length : -5.131667e+013
Total Track : 922.707
Image Space F/# : 33.57586
Paraxial Working F/# : 2405.249
Working F/# : 2406.073
Image Space NA : 0.0002078787
Object Space NA : 0.01489
Stop Radius : 0.1024682
Paraxial Image Height : 52.00792
Paraxial Magnification : 71.63625
Entrance Pupil Diameter : 2.97833e+008
Entrance Pupil Position : 1e+010
Exit Pupil Diameter : 4157574
Exit Pupil Position : 1e+010
Field Type : Object height in Millimeters

Maximum Radial Field : 0.726
Primary Wavelength : 1.475 μm
Lens Units : Millimeters
Angular Magnification : -1.911541e-007

Fields : 5
Field Type: Object height in Millimeters

#	X-Value	Y-Value	Weight
1	0.000000	0.000000	100.000000
2	-0.726000	0.000000	50.000000
3	0.726000	0.000000	50.000000
4	0.000000	-0.726000	50.000000
5	0.000000	0.726000	50.000000

Vignetting Factors

#	VDX	VDY	VCX	VCY	VAN
1	0.000000	0.000000	0.000000	0.000000	0.000000
2	0.000000	0.000000	0.000000	0.000000	0.000000
3	0.000000	0.000000	0.000000	0.000000	0.000000
4	0.000000	0.000000	0.000000	0.000000	0.000000
5	0.000000	0.000000	0.000000	0.000000	0.000000

Wavelengths : 5
Units: μm

#	Value	Weight
1	1.475000	1.000000
2	1.800000	10.000000
3	2.200000	1.000000
4	2.400000	1.000000
5	1.170000	1.000000

SURFACE DATA SUMMARY:

Surf	Type	Radius	Thickness	Glass	Diameter	Conic	Comment
OBJ	STANDARD	Infinity	6.880918		1.452	0	
STO	STANDARD	6.773085	2	BAF2H120	10	0	
2	STANDARD	-6.806842	6.877347		10	0	
3	STANDARD	Infinity	138.416		0.2444866	0	
4	STANDARD	441.2625	5	BAF2H120	30	0	
5	STANDARD	-77.74181	140.8071		30	0	
6	STANDARD	Infinity	59.90376		27.14098	0	
7	STANDARD	103.7206	8	BAF2H120	30	0	
8	STANDARD	-41.10468	62.30034		30	0	
9	STANDARD	Infinity	237.425		4.199363	0	

10 STANDARD	220.9268	25	BAF2H120	130	0	
11 STANDARD	-232.6481	236.9774		130	0	
IMA STANDARD	Infinity			104.897	0	

8.3 IZ Scale Changer

System/Prescription Data

File:
\\.psf\Home\Documents\Dropbox\KNGAO_instrument_only_wifs_scalechanger_iz_2ndrelayfixed.ZMX

Title: Scale changing optics, IZ, DAVINCI IFS
Date : MON APR 12 2010
Configuration 3 of 3

LENS NOTES:
config 1 800
config 2 801
config 3 802

GENERAL LENS DATA:

Surfaces : 12
Stop : 1
System Aperture : Object Space NA = 0.01489
Telecentric Object Space: On
Glass Catalogs : MISC SCHOTT HERAEUS OHARA INFRARED MOSFIRE
Ray Aiming : Off
Apodization : Uniform, factor = 0.00000E+000
Temperature (C) : 2.00000E+001
Pressure (ATM) : 1.00000E+000
Adjust Index Data To Environment : Off
Effective Focal Length : 1e+010 (in air at system temperature and pressure)
Effective Focal Length : 1e+010 (in image space)
Back Focal Length : -1.697669e+012
Total Track : 895.2639
Image Space F/# : 33.57586
Paraxial Working F/# : 437.4752
Working F/# : 437.6136
Image Space NA : 0.001142921
Object Space NA : 0.01489
Stop Radius : 0.5126384
Paraxial Image Height : 47.29692
Paraxial Magnification : 13.02945
Entrance Pupil Diameter : 2.97833e+008

Entrance Pupil Position : 1e+010
Exit Pupil Diameter : 2.285844e+007
Exit Pupil Position : 1e+010
Field Type : Object height in Millimeters
Maximum Radial Field : 3.63
Primary Wavelength : 0.85211 μm
Lens Units : Millimeters
Angular Magnification : -0

Fields : 5
Field Type: Object height in Millimeters

#	X-Value	Y-Value	Weight
1	0.000000	0.000000	100.000000
2	-3.630000	0.000000	50.000000
3	3.630000	0.000000	50.000000
4	0.000000	-3.630000	50.000000
5	0.000000	3.630000	50.000000

Vignetting Factors

#	VDX	VDY	VCX	VCY	VAN
1	0.000000	0.000000	0.000000	0.000000	0.000000
2	0.000000	0.000000	0.000000	0.000000	0.000000
3	0.000000	0.000000	0.000000	0.000000	0.000000
4	0.000000	0.000000	0.000000	0.000000	0.000000
5	0.000000	0.000000	0.000000	0.000000	0.000000

Wavelengths : 2
Units: μm

#	Value	Weight
1	0.852110	10.000000
2	0.970000	1.000000

SURFACE DATA SUMMARY:

Surf	Type	Radius	Thickness	Glass	Diameter	Conic	Comment
OBJ	STANDARD	Infinity	34.42455		7.26	0	
STO	STANDARD	47.25033	2	BAF2H120	8.290703	0	
2	STANDARD	-25.45857	34.83521		8.237032	0	
3	STANDARD	Infinity	112.0518		1.193918	0	
4	STANDARD	96.13798	5	BAF2H120	24.77758	0	
5	STANDARD	-119.5316	111.6808		24.97922	0	
6	STANDARD	Infinity	57.35812		23.56845	0	
7	STANDARD	100.2095	8	BAF2H120	23.75944	0	
8	STANDARD	-39.73282	59.74962		23.3489	0	
9	STANDARD	Infinity	240.8639		3.336565	0	

10 STANDARD	205.3838	25	BAF2H120	107.1103	0
11 STANDARD	-263.4573	238.7245		108.3315	0
IMA STANDARD	Infinity			95.82192	0

9 Appendix B: Atmosphere and System Transmissions

	Cut-on, nm	Cut-off, nm	Atmosphere	Atmosphere, average	AO system	AO system, average
I band						
S, P	700		91.37%	92.26%	44.45%	51.05%
S, P		853	93.15%		57.64%	
Z band						
S	855		93.15%	96.56%	57.64%	57.98%
S		1050	99.97%		58.33%	
P	818		92.90%	96.04%	55.59%	57.57%
P		922	99.18%		59.54%	
Y band						
S	970		99.31%	92.02%	61.08%	59.84%
S		1120	84.74%		58.60%	
P	970		99.31%	99.63%	61.08%	60.51%
P		1070	99.96%		59.93%	
J band						
S	1100		98.72%	63.67%	58.65%	58.56%
S		1400	28.62%		58.47%	
P	1170		99.22%	97.76%	57.48%	57.90%
P		1330	96.30%		58.31%	
H band						
S	1475		96.58%	86.40%	59.59%	61.15%
S		1825	76.23%		62.70%	
P	1490		95.38%	97.10%	59.75%	60.76%
P		1780	98.82%		61.78%	
K band						
S	2000		63.46%	79.31%	62.81%	62.25%
S		2400	95.16%		61.69%	
P	2030		97.19%	90.73%	62.73%	62.23%
P		2370	84.27%		61.73%	

Table 14: Atmosphere and AO system throughput estimates

Cut-on and cut-off wavelengths for spectroscopic (S) and photometric (P) bands shown in nm, green highlighted values used for background predictions.

	Cut-on, nm	Cut-off, nm	R ave. %	3 ref. %
I band	700	853	86.99	65.82
Z band	855	1050	91.58	76.81
Y band	970	1120	94.42	84.18
J band	1100	1400	96.22	89.09
H band	1475	1825	97.13	91.62
K band	2000	2400	97.35	92.26

Table 15: Keck telescope transmission